



Alkylation for removing trace olefins from reforming aromatics over novel $\text{Al}_2\text{O}_3@\text{SO}_4^{2-}/\text{ZrO}_2$ catalysts derived from the ZrO_2 -coated $\gamma\text{-Al}_2\text{O}_3$ strategy

Sitan Wang, Xuan Meng, Naiwang Liu ^{*}, Li Shi ^{*}

The State Key Laboratory of Chemical Engineering, East China University of Science and Technology, Shanghai 200237, People's Republic of China



ARTICLE INFO

Keywords:

Sulfated zirconia
 $\text{Al}_2\text{O}_3@\text{SO}_4^{2-}/\text{ZrO}_2$
 Coating structure
 Alkylation
 Aromatics
 Olefins removal

ABSTRACT

Sulfated zirconia, as a promising catalyst in various acid-catalytic reactions, still suffer from unsatisfactory catalytic stability and regeneration performance due to severe leaching of sulfur species, while aluminum modification can effectively overcome these drawbacks. Unfortunately, the limited acceptability of aluminum content by co-precipitation and milling methods remains a critical issue. Herein, an effective strategy of coating sulfated zirconia on the surface of $\gamma\text{-Al}_2\text{O}_3$ was developed to synthesize the novel $\text{Al}_2\text{O}_3@\text{SO}_4^{2-}/\text{ZrO}_2$ catalyst with high aluminum content. The synthesis variables were investigated and systematically optimized. The structural and acidic properties of $\text{Al}_2\text{O}_3@\text{SO}_4^{2-}/\text{ZrO}_2$ were determined by XRD, HR-TEM equipped with EDX, N_2 adsorption-desorption isotherms, EA, FT-IR, $\text{NH}_3\text{-TPD}$ and Py-FTIR. Results indicated that the unique structure constructed by sulfated zirconia coated on $\gamma\text{-Al}_2\text{O}_3$ not only realized the stabilization of favorable tetragonal zirconia phase even at exceedingly high aluminum content but also promoted Brønsted acid sites. Accordingly, the optimal $\text{Al}_2\text{O}_3@\text{SO}_4^{2-}/\text{ZrO}_2\text{-50\%}$ performed outstanding catalytic activity and stability, given the olefins conversion of 98%-75% during the continuous reaction experiment. Owing to the alleviation of sulfur loss by Al-promoting effects, excellent regeneration performance, with olefins conversion only slightly declining after 4 consecutive reaction-regeneration cycles, was also obtained. The mechanistic pathway for the alkylation of olefins with aromatics over $\text{Al}_2\text{O}_3@\text{SO}_4^{2-}/\text{ZrO}_2$ was also investigated and proposed by GC-MS analysis.

1. Introduction

Aromatics (benzene, toluene and xylene), as primary organic raw materials in petrochemical processes, are of significant importance to the fine-chemical, military and pharmaceutical industries [1]. Naphtha reforming and thermal cracking are the two main processes for producing these aromatic hydrocarbons. However, undesirable olefin impurities are inevitably contained in aromatic streams since the inherent limitation of manufacturing technology. These olefins with high chemical activities tend to oligomerize to form gums and other by-products, leading to adverse effects on downstream technological processes of aromatic streams. Hence, removing these detrimental trace olefins from aromatics before their application in subsequent processing is indispensable.

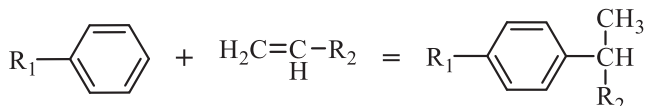
Two feasible methods have been adopted for removing trace olefins from aromatics. One method is catalytic hydrogenation treatment, in which olefins can effectively saturate by reacting with hydrogen in the presence of catalysts [2,3]. However, the elimination of olefins can be accompanied by the loss of aromatics as the depth of hydrogenation is

challenging to control. Besides, harsh reaction conditions of hydro-treating impose high requirements on equipment. Another solution for olefins removal is via alkylation of olefins with specific aromatics (**Scheme 1**) over the acid catalyst to generate long-chain alkylbenzenes with a high boiling point, which can be removed in the subsequent distillation unit [4]. In view of the mild operating conditions and slight loss of aromatics, this solution is considered more attractive. Based on the principle of alkylation, clay treatment with activated clay as the catalyst is the most predominant process for olefins removal in chemical industries [3–5]. However, limited by their inadequate acid sites and poor thermal stability, clay catalysts exhibit drawbacks of limited lifetime and poor regeneration performance, necessitating frequent catalyst replacement operations. In addition, the solid disposal and landfilling of deactivated clay as hazardous waste will cause severe environmental pollution, which can not satisfy the increasingly stringent environmental restrictions [2,3,6]. Therefore, developing alternative catalysts to overcome these drawbacks and improve the process for the purification of aromatics has been of keen interest over past decades.

Through continuous efforts of our group and other researchers,

* Corresponding authors.

E-mail addresses: liunw@ecust.edu.cn (N. Liu), yishi@ecust.edu.cn (L. Shi).



Scheme 1. Diagram of alkylation between aromatics and olefins.

numerous efficient acid catalysts, such as modified clay [2,3,7–9], zeolites [10–12], acidic ionic liquids [13,14] and sulfated zirconia [15–17], have been developed and extensively investigated. The clay catalyst with modification of $ZnCl_2$, $AlCl_3$ or $CoCl_2$ displays improved catalytic activity and lifetime than pristine activated clay, but difficulties in catalyst regeneration and disposal of waste catalysts still persist as formidable drawbacks. Benefiting from the specific acidity and porous structures, the zeolite catalyst can perform acceptable catalytic activity as olefins conversion of 90–100% at the beginning of the reaction. Still, the rapid deactivation and unsatisfactory regeneration performance of zeolites are problematic and restrict their industrial application. Although superior catalytic performance can be obtained over acidic ionic liquids, their shortcomings of highly moisture sensitive, complex synthesis and purification process, and difficult recycling make such catalysts not suitable for practical chemical industries. Compared to these catalysts, sulfated zirconia has been considered a promising catalyst for purification of aromatic streams to substitute currently used clay-based catalysts, given its attractive advantages of excellent catalytic performance, easily recyclable, environmental friendliness, unique acid properties and so on [15,16,18–20]. The conventional method to synthesize sulfated zirconia is the hydrolysis of zirconium salt followed by post-sulfonation and calcination. Nonetheless, the resultant sulfated zirconia suffers from unsatisfactory catalytic stability and regeneration performance, resulting from low surface area, limited Brønsted acid sites and seriously leaching of active sulfur species [21–23].

Previous studies [18,21,23–27] suggest that one approach to solving these problems can be achieved by introducing Al_2O_3 into sulfated zirconia in the synthesis process. In our earlier work [18], it has been validated that incorporation of a small amount of Al into the sulfated zirconia catalyst not only promotes stabilizing catalytically active tetragonal zirconia but also enhances Brønsted acid sites and interaction between sulfur species and zirconia, which contribute to the improvement of catalytic activity and reusability of the catalyst. As demonstrated by Canton et al. [25] and Hwang et al. [26], the surface area and porosity of sulfated zirconia can also be increased by modification of Al_2O_3 , making the catalyst present more available active sites for the accessibility of reactants. Zhang et al. [23] reported that the Al-promoted sulfated zirconia shows higher catalytic activity and stability than the unpromoted catalyst driven by the role of Al promoter in increasing surface sulfur content and the ratio of Brønsted to Lewis acid sites. Reddy et al. [27] pointed out that the incorporation of Al into zirconia and subsequent sulfonation leads to the formation of mixed oxides with the interaction between Zr and Al atoms, which, in turn, is in favor of increasing the concentration and thermal stability of surface sulfate groups onto catalysts. Consequently, the sulfur leach of the sulfated zirconia catalyst can also be alleviated by Al introduction. Moreover, the addition amount of Al is known to significantly affect the properties and catalytic activity of Al-promoted sulfated zirconia [18,25,28]. To date, most of the strategies that have been reported for introducing Al into sulfated zirconia follow the approach of co-precipitation method or milling method. The optimal Al addition of the catalyst is limited to 5–10 mol% on account of the homogeneous distribution of Zr and Al in the synthesis process. The high addition of Al will hinder the crystallization of amorphous zirconium hydroxide to zirconia with the favorable tetragonal phase, thereby reducing catalytic performance. As reported in our recent work [18], both the crystallinity of zirconia and overall catalytic performance decrease with the increase of Al addition, meanwhile the Al-promoted sulfated zirconia catalyst with Al addition of $Al/Zr = 50$ mol% almost maintains an amorphous

phase after calcination at 650 °C. From the practical application point of view, developing the effective and stable Al-promoted sulfated zirconia with high Al content can not only make it possible to reduce the cost of the catalyst but also raise the utilization rate of active components.

Recently, Liu et al. [29] reported a new method for the synthesis of $Al_2O_3@ZrO_2$ core-shell composite nanorods with alumina as the core and zirconia as the shell by depositing zirconium species onto the boehmite nanofibers via chemical liquid deposition. Given that the Al_2O_3 is applied as the support, even in the case of exceedingly high alumina addition, Zr species deposited on the alumina by this method can still be preserved as stabilized tetragonal zirconia. By varying the ratio of Zr to Al, the acceptable loading amount of zirconia can be successfully coated on the surface of alumina. Inspired by this, a novel $Al_2O_3@SO_4^{2-}/ZrO_2$ composite catalyst with a structure composed of sulfated zirconia-coated alumina was synthesized by post-sulfonation and calcination for $Al_2O_3@ZrO_2$ composites in the present work and applied as a promising catalyst in alkylation for removing trace olefins from aromatics. The optimization of the synthesis of the $Al_2O_3@SO_4^{2-}/ZrO_2$ catalyst was systematically investigated, where four synthesis variables, including impregnation concentration (C_s), impregnation time (t_i), calcination temperature (T_c) and zirconia loading (N_{Zr}), were concerned. The optimal $Al_2O_3@SO_4^{2-}/ZrO_2$ -50% catalyst was found to perform an excellent catalytic activity and reusability even under the long reaction time, which is superior to the bulk sulfated zirconia, as well as the high-aluminum-content sulfated zirconia synthesized by the co-precipitation method or milling method. To in-depth reveal the detailed structures and surface active sites of such a novel catalyst, the $Al_2O_3@SO_4^{2-}/ZrO_2$ catalyst with different Zr loading varying from 20% to 60% was characterized by XRD, HR-TEM equipped with EDX, N_2 adsorption-desorption isotherms, EA, FT-IR, NH_3 -TPD and Py-FTIR technologies. Therefore, the fabrication mechanism and the possible assembly structure of the catalyst were proposed. Additionally, the mechanistic pathway for the alkylation of olefins with aromatics over the $Al_2O_3@SO_4^{2-}/ZrO_2$ catalyst was also investigated in detail by model reaction and GC-MS. Up to now, the high-aluminum-content Al-promoted sulfated zirconia with the maintenance of high catalytic activity is hardly reported. Herein, $Al_2O_3@SO_4^{2-}/ZrO_2$, as a type of Al-promoted sulfated zirconia with exceedingly high aluminum content, could still possess remarkable catalytic performance owing to its unique structural and acidic properties. It is valuable of our work to provide an effective strategy to develop an efficient, stable, low-cost and eco-friendly sulfated zirconia catalyst for practical industrial processes.

2. Experimental section

2.1. Chemicals and reagents

The n-butanol ($CH_3(CH_2)_3OH$, A.R.), zirconium (IV) n-butoxide ($C_{16}H_{36}O_4Zr_2$, 40 wt% in n-butanol), toluene (C_7H_8 , A.R.), m-xylene (C_8H_{10} , A.R.) and 1-octene (C_8H_{16} , A.R.) were purchased from Shanghai Macklin Biochemical Co., Ltd. Potassium bromide (KBr, A.R.), pyridine (C_5H_5N , A.R.), zirconium (IV) oxychloride octahydrate ($ZrOCl_2 \cdot 8H_2O$, A.R.) and aluminum nitrate nonahydrate ($Al(NO_3)_3 \cdot 9H_2O$, A.R.) were derived from Aladdin Reagent Co., Ltd. Ammonium hydroxide ($NH_3 \cdot H_2O$, purity of 28–30 wt%) and sulfuric acid (H_2SO_4 , G.R.) were acquired from Sinopharm Chemical Reagent Co., Ltd. Moreover, pseudo-boehmite ($AlOOH \cdot H_2O$, nano-sized white powder) was provided by Hangzhou Zhihuajie Technology Co., Ltd. These chemicals and reagents were used as received without further purification.

2.2. Synthesis of catalysts

2.2.1. Synthesis of $Al_2O_3@SO_4^{2-}/ZrO_2$ via the chemical liquid deposition method

The synthesis process of sulfated ZrO_2 -coated Al_2O_3 catalysts can be simply divided into two parts. In the first stage, to obtain the precursor,

zirconium hydroxide was coated on pseudo-boehmite via chemical liquid deposition and hydrolysis of zirconium (IV) n-butoxide. In the second stage, the sulfonation and calcination of as-synthesized precursors were carried out to obtain active $\text{Al}_2\text{O}_3@\text{SO}_4^2/\text{ZrO}_2$ catalysts. The overall synthesis procedure of the catalyst is shown in Fig. 1 and illustrated in detail as follows.

Firstly, 1 g of pseudo-boehmite powder together with 1 ml of deionized water were dispersed in 60 ml of n-butanol while stirring vigorously. Then the mixture was continuously stirred with 500 rpm at room temperature for 12 h to disperse the pseudo-boehmite nanoparticles in n-butanol thoroughly and ensure fine immobilization of preadsorbed water on their surface. After that, the calculated amount of zirconium (IV) n-butoxide was added dropwise to the resulting mixture with 300 rpm stirring at room temperature for another 15 min. The resultant white colloidal solution was then transferred into a Teflon-lined autoclave, heated to 170 °C and kept for 24 h for hydrothermal treatment. After the autoclave was cooled down to room temperature, the colloidal solution was centrifuged at 6000 rpm for 15 min to separate and collect the white precipitates. Without any washing, the collected solids were then entirely dried in an oven at 110 °C for 24 h to obtain $\text{AlOOH}@\text{Zr(OH)}_4$ composites. Subsequently, the sulfonation of the composite sample was performed via the wet-impregnation method with sulfuric acid as the sulfonating agent. The detailed procedure was 1 g of $\text{AlOOH}@\text{Zr(OH)}_4$ powder immersed in 10 ml of 0.5 mol/L H_2SO_4 solution for 1 h and stirred continuously with 500 rpm at room temperature. Afterward, the resultant solid sample was separated by filtration without washing, dried at 110 °C for 12 h and calcined at 650 °C for 3 h under dry airflow to obtain active catalysts. The catalysts synthesized according to this route were denoted as $\text{Al}_2\text{O}_3@\text{SO}_4^2/\text{ZrO}_2-N$, with N representing the molar percentage ratio of Zr/(Zr + Al). For comparison, the stand-alone $\gamma\text{-Al}_2\text{O}_3$ cat catalyst sample was obtained by calcining pseudo-boehmite nanoparticles at 650 °C. Moreover, the sample, labeled as $\text{SO}_4^2/\text{Al}_2\text{O}_3$, was synthesized by direct sulfonation of pseudo-boehmite nanoparticles with 0.5 mol/L H_2SO_4 and subsequent calcination at 650 °C for 3 h.

2.2.2. Synthesis of $\text{P-SO}_4^2/\text{ZrO}_2 + \text{Al}_2\text{O}_3$ via the co-precipitation method

The $\text{P-SO}_4^2/\text{Al}_2\text{O}_3 + \text{ZrO}_2$ catalyst was synthesized by a co-precipitation method following our previous study [18]. According to the molar percentage ratio of Zr/(Zr + Al) = 50%, the appropriate amount of zirconium (IV) oxychloride octahydrate ($\text{ZrOCl}_2\cdot 8\text{H}_2\text{O}$) together with aluminum nitrate nonahydrate ($\text{Al}(\text{NO}_3)_3\cdot 9\text{H}_2\text{O}$) were

dissolved in deionized water. Then the mixed solution was added dropwise to the aqueous ammonia solution ($\text{NH}_3\cdot\text{H}_2\text{O}$) under vigorous stirring until the pH reached 9.5. The resultant colloidal was aged in the mother solution for 12 h, followed by filtration and washing with deionized water until chloride ions were absent in the filtrate (by AgNO_3 test). After being thoroughly dried, the zirconium-aluminum hydroxide composites were sulfonated with 0.5 mol/L H_2SO_4 solution at a ratio of 10 ml/g solid sample. Subsequently, the collected solid samples were dried at 120 °C and calcined at 650 °C for 3 h to obtain the target catalyst, marked as $\text{P-SO}_4^2/\text{Al}_2\text{O}_3\text{-ZrO}_2$.

2.2.3. Synthesis of $\text{SO}_4^2/\text{ZrO}_2$

The stand-alone $\text{SO}_4^2/\text{ZrO}_2$ catalyst was also synthesized and applied as a reference catalyst sample that was not modified by aluminum. The synthesis procedure of $\text{SO}_4^2/\text{ZrO}_2$ was similar to that of the $\text{P-SO}_4^2/\text{Al}_2\text{O}_3 + \text{ZrO}_2$ catalyst, except that no $\text{Al}(\text{NO}_3)_3\cdot 9\text{H}_2\text{O}$ component was added to the $\text{ZrOCl}_2\cdot 8\text{H}_2\text{O}$ solution during the synthesis of the precursor.

2.2.4. Synthesis of $M-\text{SO}_4^2/\text{ZrO}_2 + \text{Al}_2\text{O}_3$ via the milling method

The $M-\text{SO}_4^2/\text{ZrO}_2 + \text{Al}_2\text{O}_3$ catalyst was synthesized based on a milling method, aimed at loading ZrO_2 on $\gamma\text{-Al}_2\text{O}_3$. The (Zr(OH)_4) precursors, synthesized according to the same route described above, together with an appropriate amount of pseudo-boehmite nanopowders were thoroughly ground until well mixed. Note that the molar percentage ratio of Zr/(Zr + Al) = 50% was also adopted in this synthesis process to keep the content of zirconia and alumina consistent with other samples. Then the sulfonation and calcination treatments for the resultant mixture were also performed following the same route as the synthesis of $\text{P-SO}_4^2/\text{ZrO}_2 + \text{Al}_2\text{O}_3$. The as-synthesized catalyst was named $M-\text{SO}_4^2/\text{ZrO}_2 + \text{Al}_2\text{O}_3$.

2.3. Characterization of catalysts

The X-ray diffraction (XRD) patterns of catalysts were explored by using a Bruker D8 Advance X-ray diffractometer equipped with Cu K α radiation ($\lambda = 1.54 \text{ \AA}$) operating at 40 kV and 30 mA. The measurements for the samples were performed from the 2 θ range of 6° to 80° with a step size of 0.02° and a scanning rate of 1°/min.

The surface micrographs of the catalysts were obtained by means of a JEOL JEM-2100 high-resolution transmission electron microscopy (HR-TEM) equipped with a Schottky field-emission source. Additionally, the EDS spectrum was also collected employing the X-ray energy dispersive

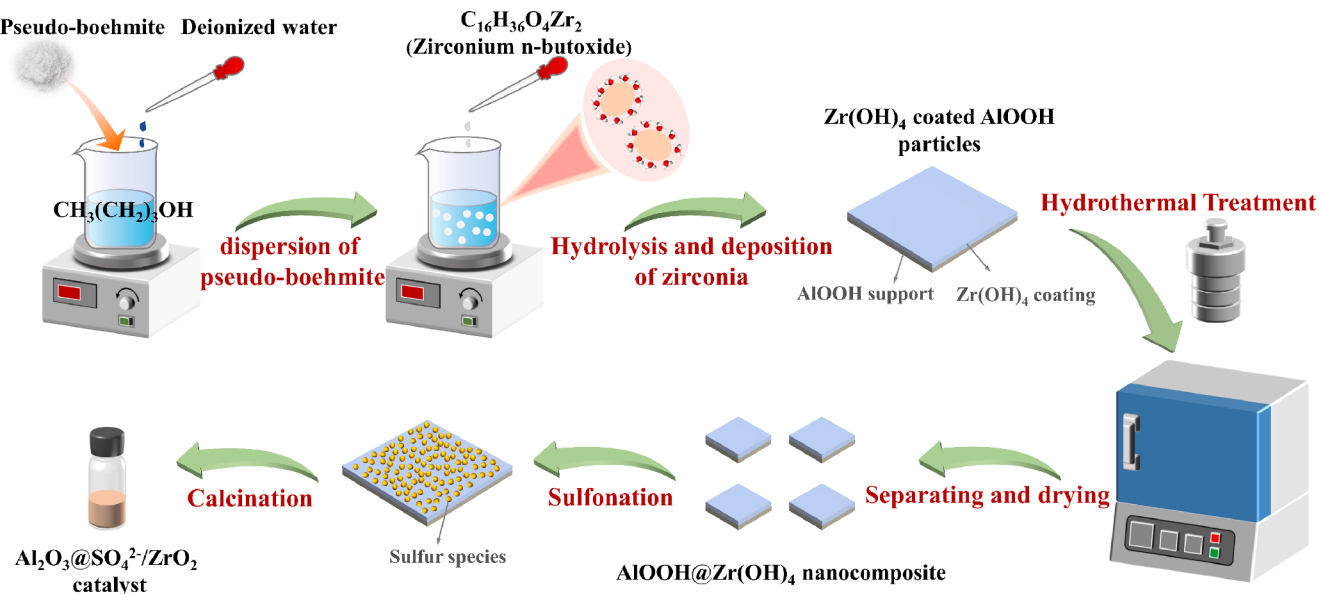


Fig. 1. Schematic of the synthesis of sulfated ZrO_2 coated Al_2O_3 composite catalysts ($\text{Al}_2\text{O}_3@\text{SO}_4^2/\text{ZrO}_2$).

spectrometer (EDAX, American) to determine the elemental distribution mapping of the catalyst.

The specific surface areas, total pore volumes and average pore sizes of as-synthesized catalysts were determined by carrying out the adsorption and desorption measurements of N₂ at -196 °C on a JW-ZQ200 material suction and desorption instrument from JWGB (Beijing JWGB Sci & Tech Co., Ltd.). To remove physically adsorbed water on the sample, the sample was degassed in situ at 350 °C for 3 h before each detection of the N₂ adsorption-desorption isotherm. The specific surface areas were calculated over the relative pressure (P/P₀) range of 0.05–0.30 by applying the Brunauer-Emmett-Teller (BET) method, and the total pore volumes of catalysts were estimated at the P/P₀ of 0.99. Mesopore properties of the catalyst, such as average pore sizes and pore size distributions, were derived from the desorption branch of the isotherm by adopting the Barren-Joyner-Halenda method.

In order to investigate the functional groups of the catalyst, a Nicolet IS-10 infrared spectrometer was employed to detect and collect the Fourier transform infrared (FT-IR) spectra of these catalysts. Before each measurement, self-supporting wafers were prepared by thoroughly mixing the finely ground catalyst samples with dried KBr powder at a fixed mass ratio (1:100) and then pressing in a compression die.

The actual content of sulfur retained on the as-synthesized catalysts was measured using CHNS analysis performed on the VARIO EL III elemental analyzer. Thermogravimetry analysis (TGA) of catalysts was investigated by a TA Instrument Q600 Analyser. The 50 mg of samples were heated from room temperature to 800 °C at a rate of 10 °C/min under a constant air flow at 30 ml/min.

The acidity of the catalysts was estimated by temperature programmed desorption of ammonia (NH₃-TPD) measurements, which were carried out on an Auto Chem 2910 instrument, and a TP-5076 thermal conductivity detector (TCD) was used to collect the ammonia desorption profile. In a typical run, 50 mg of the sample was placed in the quartz tube and degassed at 300 °C for 2 h under He flow with a constant flow rate of 30 ml/min to remove adsorbed components. After cooling down to 50 °C, the sample was exposed to 10% NH₃/He for 30 min to adsorb NH₃ saturatedly. To remove the weakly physisorbed NH₃, NH₃/He was substituted by He, and the sample was then purged at 50 °C for 1 h under He flow. After that, the temperature was increased from 50 °C to 700 °C at a constant rate of 10 °C/min, while the NH₃-TPD profile was analyzed and recorded with a thermal conductivity detector.

Besides, the Brønsted-Lewis acid character of the catalysts was determined by pyridine-adsorbed FT-IR (Py-FTIR) measurements. The spectra of each pyridine-adsorbed sample were recorded on a Nicolet IS-10 spectrometer equipped with an in situ vacuum adsorption system. Prior to analysis, the self-supporting wafer pressed from the sample powder was placed into an in-situ vacuum cell and degassed at 380 °C

for 2 h. After cooling down to 80 °C, pyridine vapor was introduced into the cell for wafer adsorption of pyridine for 30 min. Then the system was heated to 200 °C or 450 °C and kept for 15 min, respectively, to detect the Py-IR spectra of the catalysts.

To figure out the reaction mechanism over the catalyst, the reaction products in this work were identified by GC-MS technology. The measurement was conducted on Agilent PY/GC-MS/7890A-5975C equipped with the HP-5 MS column (30 m × 250 μm, i.d. × 0.25 μm).

2.4. Evaluation of catalytic performance

For studying the effect of synthesis variables on the catalytic performances to optimize the synthesis procedure, the catalytic performance evaluation of the catalyst was carried out in a stainless steel autoclave equipped with an overhead mechanical stirrer, temperature controller and sampling dip tube. The schematic diagram of the batch reactor system is shown in Fig. 2a. In a typical procedure, 26.04 g of reforming aromatics feedstock and 0.65 g of as-synthesized catalyst were fed to the reactor. Then the reactor was sealed and purged with N₂ for 5 min to replace the air in the headspace, followed by being filled again with N₂ and heated until the pressure and temperature reached 1.0Mpa and 175 °C, respectively. Next, the reactor stirring commenced at a rate of 500 rpm/min, with reactions carried out for 2 h. After the reaction, aromatic products were collected and analyzed using a Bromine Index Analyzer (LC-6).

The Bromine index (BI), defined as the number of milligrams of bromine that would react with trace olefins in 100 g of the aromatics sample, is applied as an indicator to determine the olefin content in aromatics. Therefore, the conversion of olefins in this study was calculated based on the following equation:

$$\text{Conversion} = \left(1 - \frac{\text{BI}_t / \text{BI}_0}{\text{BI}_0} \right) \times 100\%$$

where BI₀ is the Bromine index of the aromatic feedstock and BI_t is used to indicate the Bromine index of the aromatic product.

In order to ensure reproducibility, the catalytic performance experiment for each sample was repeated 3 times and the conversion was determined by the average of the results obtained from three tests. The raw reforming aromatics originated from the catalytic reforming unit of Sinopec Zhenhai Refining & Chemical Company. The detailed components are provided in Table 1, and the BI of the reforming aromatic hydrocarbons is 1200 ~ 1300 mg Br/(100 g).

To further evaluate the catalytic stability and reusability of the optimized catalyst, a fixed-bed tubular microreactor system was adopted to conduct catalytic performance experiments. Fig. 2b shows the schematic diagram of the fixed-bed tubular microreactor device. The reactor

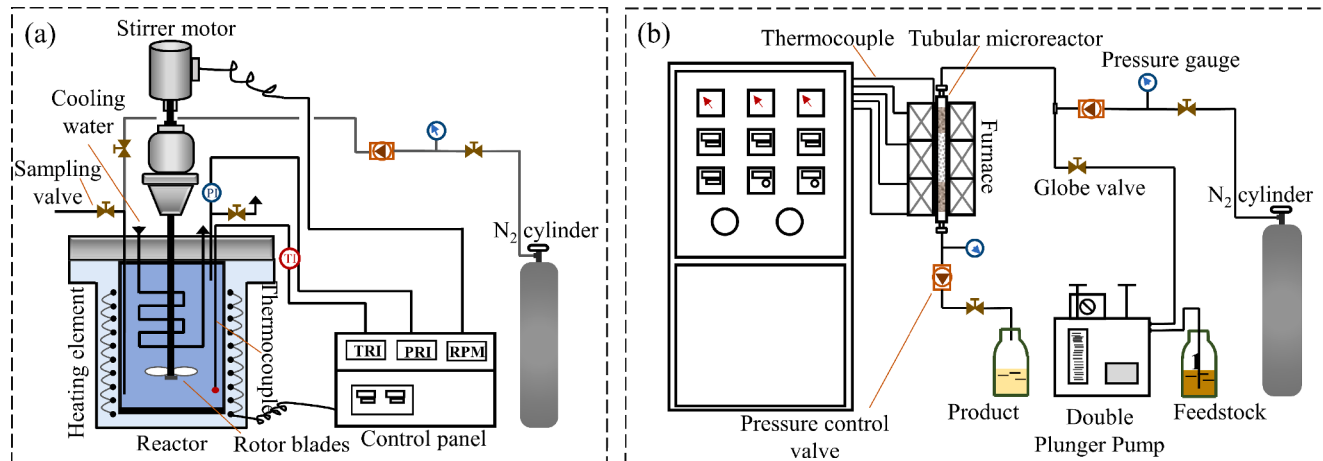


Fig. 2. Schematic diagram of the experimental apparatus. (a) batch reactor device; (b) fixed-bed tubular microreactor device.

Table 1
Components of the aromatic hydrocarbons applied as feedstock.

Component	Average content (wt %)
non-aromatics	2.53
benzene	0.01
toluene	0.04
ethylbenzene	6.47
p-xylene	8.75
m-xylene	18.74
o-xylene	12.26
C ₉ and C ₉ ⁺	51.20

bed was constructed as a sandwich structure with the filling layer of quartz sand/catalyst sample/quartz sand from top to bottom, where the catalyst sample layer was loaded with 1.72 g of dried catalyst (40–60 mesh) in each experiment. After purging the reaction system with N₂ for 1 h, the reforming aromatics feedstock was pumped into the reactor at a flow rate of 0.5 ml/min (liquid hourly space velocity, LHSV = 30 h⁻¹). Then the reaction was performed at 175 °C and 1.0 MPa. Product samples were periodically collected for analysis by the LC-6 Bromine Index Analyzer to calculate olefins conversion.

3. Results and discussion

3.1. Optimization of synthesis variables in the synthesis of Al₂O₃@SO₄²⁻/ZrO₂ catalysts

3.1.1. Effect of synthesis variables on the catalytic performances

Typically, for synthesizing sulfated zirconia catalysts, the concentration of the sulfonating reagent for treatment, the sulfonation time, the calcination temperature and the active component content are crucial factors that affect the catalytic performances of resultant catalysts [20,30–32]. Thus, to optimize the synthesis procedure of Al₂O₃@SO₄²⁻/ZrO₂ catalysts, different synthesis variables such as sulfonation concentration (C_s), sulfonation time (t_i), calcination temperature (T_c), and zirconia loading (N_{Zr}) were concerned in the current study. A series of control experiments were conducted to investigate the effect of these variables on catalytic performance for olefins removal. The results are summarized and listed in Fig. 3.

As depicted in Fig. 3a, the conversion of olefins obtained by Al₂O₃@SO₄²⁻/ZrO₂ catalysts increased from 43.82% to 93.78% within the sulfonation concentration ranging from 0.1 mol/L to 0.5 mol/L, and then decreased from 93.78% to 8.47% with further aggrandizing the concentration of H₂SO₄ solution used in sulfonation treatment from 0.5 mol/L to 2 mol/L. The results demonstrated that sulfonation of the precursor with a low concentration of H₂SO₄ solution was insufficient to invigorate the superior catalytic activity of the catalyst, which might be

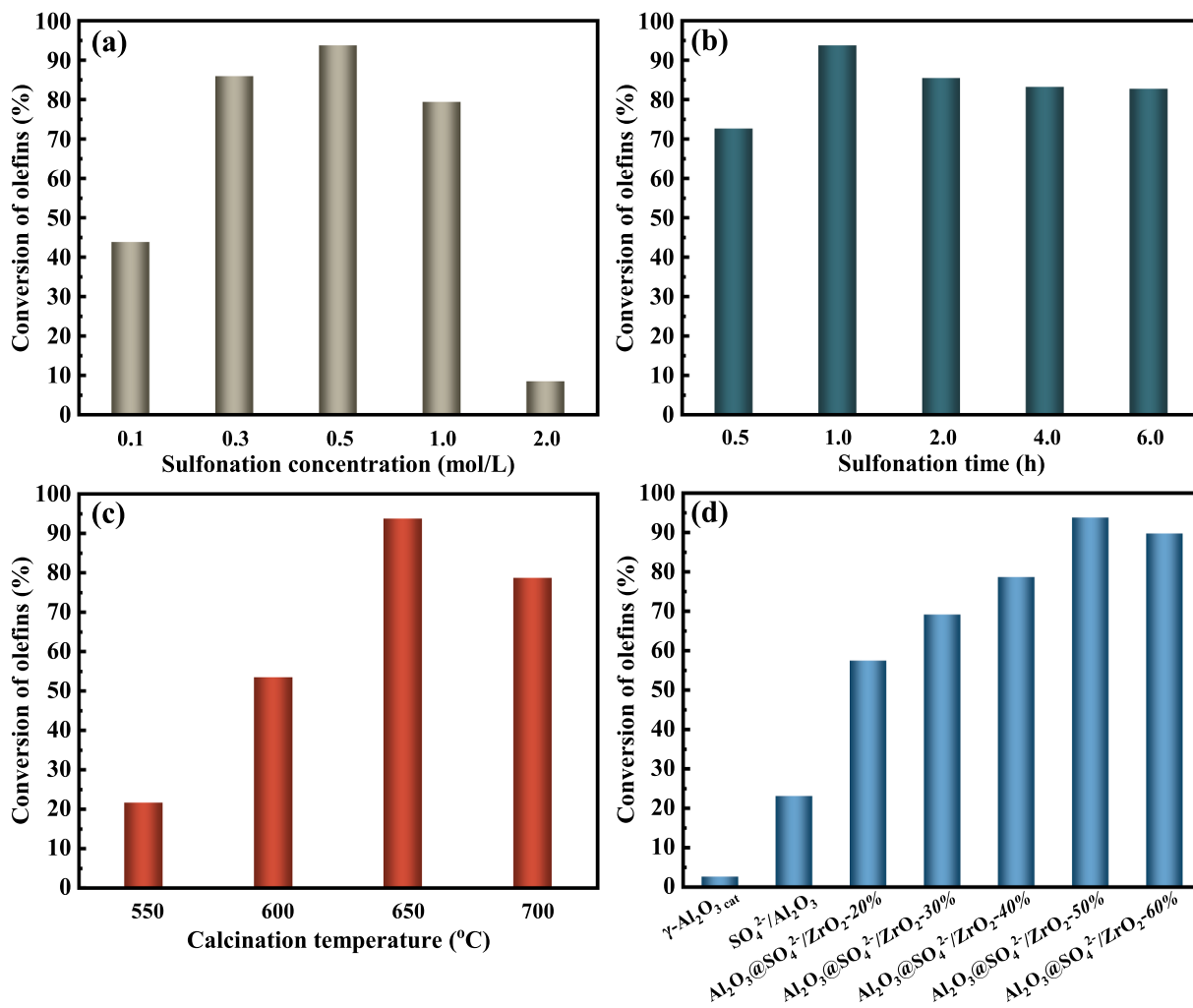


Fig. 3. The catalytic performance in removing trace olefins from aromatics of as-synthesized catalysts. (a) Effect of sulfonation concentration (t_i = 1 h, T_c = 650 °C, N_{Zr} = 50%); (b) Effect of sulfonation time (C_s = 0.5 mol/L, T_c = 650 °C, N_{Zr} = 50%); (c) Effect of calcination temperature (C_s = 0.5 mol/L, t_i = 1 h, N_{Zr} = 50%); (d) Effect of zirconia loading (C_s = 0.5 mol/L, t_i = 1 h, T_c = 650 °C).

attributed to the low active sulfur species loading and acidity caused by insufficient sulfonation. Notably, a dramatic decrease in olefin conversion was observed when the H_2SO_4 concentration increased from 1 mol/L to 2 mol/L. Similar findings were made in previous studies [17,20,33] that $Zr(OH)_2SO_4$ and $Zr(SO_4)_2$ are present in the catalyst synthesized by the treatment of sulfonation reagent with excessive concentration, leading to the weakening of acid sites and catalytic activity eventually. The super acidity and excellent catalytic performance of such the catalyst could be invigorated by sulfonation with an appropriate concentration of the sulfonation reagent (H_2SO_4 solution). In contrast, an excessive concentration of the sulfonation reagent adopted in the synthesis process would aggravate salifying zirconium species of the catalyst to a certain extent, thus the active sites and overall catalytic performance of the resulting catalysts were negatively affected. It was observed from Fig. 3b that the catalytic activity was dramatically improved by increasing the sulfonation time from 0.5 h to 1 h and decreased slightly with the further prolongation of sulfonation time. The conversion of olefins decreased from 93.78% to 82.70% with sulfonation time increased from 1 h to 6 h, which was negligible compared to the effect of increasing sulfonation concentration on the catalytic performance. It indicated that an impregnation time of 1 h adopted in the synthesis procedure was sufficient, and the longer sulfonation time performed a slight effect on the catalytic performance for olefins removal of as-synthesized catalysts in this study. Fig. 3c shows that the conversion of olefins progressively increased from 21.61% to 93.78% within the calcination temperature ranging from 550 °C to 650 °C and decreased with a further increase in the calcination temperature to 700 °C. The maximum conversion of olefins was obtained over the $Al_2O_3@SO_4^2-/ZrO_2$ catalyst synthesized by calcining at 650 °C. Such weakening in the catalytic activity of the catalyst initiated by increasing calcination temperature to 700 °C might be attributed to the reduction of acidity caused by the decomposition of surface sulfates, as the sulfur species retained on the sulfated zirconia catalyst will decompose at the temperature above 650 °C [19,23,34,35]. Moreover, in terms of the sulfated zirconia-coated catalyst, the zirconia loading of as-synthesized catalysts also played an essential role in affecting the catalytic performance, as suggested in Fig. 3d. The catalytic performance evaluations for $\gamma-Al_2O_3$ cat and SO_4^2-/Al_2O_3 were first performed, aiming to determine the contribution of the support to this reaction. The results showed that both samples exhibited poor catalytic activity. However, the olefins conversion obtained in the presence of $Al_2O_3@SO_4^2-/ZrO_2$ -20% was 34.32% higher than that performed by SO_4^2-/Al_2O_3 . Furthermore, it was noticeable that the catalytic performance was significantly improved with the $Al_2O_3@SO_4^2-/ZrO_2$ composite sample applied as the catalyst, indicating the excellent catalytic activity contributed by the sulfated zirconia component coated on the $\gamma-Al_2O_3$ support. As the zirconia loading increased from 20% to 50%, the catalytic activity of the catalyst

was continuously enhanced. The conversion of olefins reached a maximum of 93.78% over the $Al_2O_3@SO_4^2-/ZrO_2$ -50% catalyst. Then the conversion was slightly decreased with a further increase of the zirconia loading to 60%, where a decrement of 4.10% was observed.

In addition, further optimization of synthesis variables for the $Al_2O_3@SO_4^2-/ZrO_2$ composite catalyst was carried out by conducting an orthogonal experiment based on the $L_9(3^4)$ strategy. As in the above study, four synthesis variables (C_s , t_i , T_c and N_{Zr}) as influencing factors were considered with three levels. The catalytic performance of the catalyst was also evaluated by applying in removing trace olefins from aromatics, and the reaction conditions were the same as before. The detailed results are summarized in Table 2. Meanwhile, the k_i ($i = 1, 2, 3$) index was calculated according to the average value of olefins conversion at a certain level for each influencing factor, in which the higher the k_i index value was, the more favorable the corresponding level was for the catalytic performance of as-synthesized catalysts [36]. As presented in Table 2, it demonstrated that $C_s = 0.5$ mol/L, $t_i = 1$ h, $T_c = 650$ °C, and $N_{Zr} = 50\%$ corresponded to the optimal sulfonation concentration, the optimal sulfonation time, the optimal calcination temperature, and the optimal zirconia loading, respectively. The results derived from the orthogonal experiment were consistent with those clarified in Fig. 2. Therefore, it could be concluded that the optimal synthesis procedure for the novel $Al_2O_3@SO_4^2-/ZrO_2$ composite catalyst guided by the synthesis variables that have been investigated in the present study was as follows: $AlOOH@Zr(OH)_4$ precursor with zirconia loading of 50% was impregnated in 0.5 mol/L H_2SO_4 solution for 1 h to conduct sulfonation treatment and then calcined at 650 °C to obtain the active catalyst. Given the improved catalytic performance of the $Al_2O_3@SO_4^2-/ZrO_2$ catalyst, it is necessary to investigate the effect of zirconia loading on the physicochemical properties of as-synthesized catalysts in-depth, which contributes to figuring out the formation mechanism and the origin of outstanding catalytic activity of such the novel sulfated zirconia coated catalyst.

3.1.2. Effect of zirconia loading on the physicochemical properties

The crystalline structure of the $Al_2O_3@SO_4^2-/ZrO_2$ composite sample, as well as two Al_2O_3 support samples, was explored by X-ray diffraction measurement. As presented in Fig. 4, the XRD pattern of the $\gamma-Al_2O_3$ cat sample showed characteristic peaks at $2\theta = 37.7^\circ$, 45.8° and 66.8° , which were attributed to the diffractions from (311), (400) and (440) planes of $\gamma-Al_2O_3$ ($\gamma-Al_2O_3$, PDF#77-0403), respectively. It indicated that the amorphous pristine pseudo-boehmite nanoparticles were transformed into the sample with the crystalline structure of $\gamma-Al_2O_3$ after calcination at 650 °C. Likewise, the XRD pattern of SO_4^2-/Al_2O_3 was almost identical to that of the $\gamma-Al_2O_3$ cat sample with $\gamma-Al_2O_3$ characteristic structure, revealing that the sulfonation treatment barely affected the crystalline phase of the resulting support samples. For

Table 2
Optimization of synthesis variables for the $Al_2O_3@SO_4^2-/ZrO_2$ catalyst based on $L_9(3^4)$ orthogonal experiment.

Experiment number	Influencing factors				Conversion (%)
	Sulfonation concentration (mol/L)	Sulfonation time (h)	Calcination temperature (°C)	Molar ratio of Zr/(Zr + Al) (%)	
1	0.5	1	600	40	51.04
2	0.5	2	650	50	85.48
3	0.5	4	700	60	67.90
4	1.0	1	650	60	75.52
5	1.0	2	700	40	45.96
6	1.0	4	600	50	38.97
7	2.0	1	700	50	40.48
8	2.0	2	600	60	12.03
9	2.0	4	650	40	5.93
Index					
k_1	68.14	55.61	34.01	34.31	
k_2	53.42	47.82	55.58	54.98	
k_3	19.48	37.60	51.45	51.75	

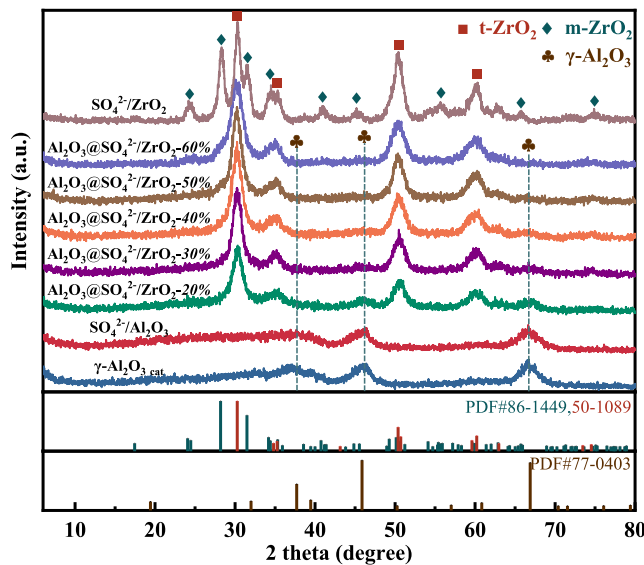


Fig. 4. Powder XRD patterns of Al_2O_3 support samples and $\text{Al}_2\text{O}_3@\text{SO}_4^{2-}/\text{ZrO}_2$ catalysts with different zirconia loading.

$\text{Al}_2\text{O}_3@\text{SO}_4^{2-}/\text{ZrO}_2$ composite samples, it was evident that the characteristic structural peaks appeared at around $2\theta = 30.3^\circ, 35.3^\circ, 50.4^\circ$ and 60.2° , corresponding to the diffractions from $(0\ 1\ 1)$, $(1\ 1\ 0)$, $(1\ 1\ 2)$ and $(1\ 2\ 1)$ planes of tetragonal zirconia (t-ZrO_2 , PDF#50-1089), respectively. Accordingly, as expected, the zirconia phase was successfully introduced into the composite catalysts. From XRD patterns in Fig. 4, it was worth noting that the intensities of the diffraction peaks of t-ZrO_2 progressively enhanced with the increase of zirconia loading from 20% to 60%, whereas the diffraction peaks attributed to $\gamma\text{-Al}_2\text{O}_3$ were reduced gradually. The characteristic structural peaks corresponding to $\gamma\text{-Al}_2\text{O}_3$ were barely undetectable in $\text{Al}_2\text{O}_3@\text{SO}_4^{2-}/\text{ZrO}_2$ catalysts with above 40% zirconia loading. On the one hand, the introduction of zirconia caused a decrease in the relative concentration of $\gamma\text{-Al}_2\text{O}_3$. On the other hand, more and more zirconia species were coated on the surface of $\gamma\text{-Al}_2\text{O}_3$ support, blocking the X-ray from reaching the $\gamma\text{-Al}_2\text{O}_3$ structure. In addition, no characteristic peaks affiliated with monoclinic zirconia (m-ZrO_2 , PDF#86-1449) were detected in all these $\text{Al}_2\text{O}_3@\text{SO}_4^{2-}/\text{ZrO}_2$ catalysts. Instead, the XRD pattern of the stand-alone $\text{SO}_4^{2-}/\text{ZrO}_2$ synthesized by the conventional method approved that the sample presented a mixed crystalline phase constructed by both m-ZrO_2 and t-ZrO_2 phase, which was in accordance with our previous study [16,18]. The result implied that the transformation of zirconia from the metastable tetragonal phase to the monoclinic phase was inhibited by coating zirconia on the surface of $\gamma\text{-Al}_2\text{O}_3$. It has been reported that the reduction in the crystallite size of zirconia is favorable for the stabilization of the metastable tetragonal phase [37–39]. As provided in Table 3, compared to $\text{SO}_4^{2-}/\text{ZrO}_2$ with crystallite sizes of 11.7 nm, all these $\text{Al}_2\text{O}_3@\text{SO}_4^{2-}/\text{ZrO}_2$ catalysts with various zirconia loading ranging from 20% to 60% exhibited much smaller main crystallite sizes varying

from 5.2 nm to 6.7 nm. The advancing and overgrowth of crystal boundaries of zirconia particles dispersed on the support surface were restricted owing to the interaction between Al_2O_3 species and ZrO_2 species, driving particles presented as small crystal size, which in turn stabilized the metastable tetragonal phase. Studies [18,24,40] suggested that the better catalytic activity of the sulfated zirconia catalyst highly depends on the metastable tetragonal zirconia phase of the catalyst. The $\text{Al}_2\text{O}_3@\text{SO}_4^{2-}/\text{ZrO}_2$ catalyst appeared the crystalline structure with all Zr-related components crystallizing into the tetragonal phase, which might account for the outstanding catalytic performance of such the catalyst.

The morphologies of the $\text{Al}_2\text{O}_3@\text{SO}_4^{2-}/\text{ZrO}_2$ catalyst and the $\text{SO}_4^{2-}/\text{Al}_2\text{O}_3$ sample were determined by HR-TEM technology. The stand-alone $\text{SO}_4^{2-}/\text{ZrO}_2$ catalyst was also characterized for comparison with $\text{Al}_2\text{O}_3@\text{SO}_4^{2-}/\text{ZrO}_2$. The representative TEM images of these samples are provided in Fig. 5. Fig. 5a and 5b show that the $\text{SO}_4^{2-}/\text{Al}_2\text{O}_3$ sample displayed a typical stacking structure with clusters of $\gamma\text{-Al}_2\text{O}_3$ nanofibers interlaced and connected together. Obviously, the $\text{Al}_2\text{O}_3@\text{SO}_4^{2-}/\text{ZrO}_2$ catalyst exhibited significant differences in morphology from the $\text{SO}_4^{2-}/\text{Al}_2\text{O}_3$ sample. As depicted in Fig. 5c ~ 5 g, fiber-like morphology attributed to $\gamma\text{-Al}_2\text{O}_3$ nanofibers gradually became invisible on the morphology of $\text{Al}_2\text{O}_3@\text{SO}_4^{2-}/\text{ZrO}_2$ catalysts and transformed into a new morphology with irregular square nanoparticles covering the surface of $\gamma\text{-Al}_2\text{O}_3$ nanofibers as the support, which could be owing to the coating of zirconia particles. Besides, it could be observed that the support surface tended to be more sufficiently covered by these nanoparticles as the zirconia loading increased, and the outer surface of $\gamma\text{-Al}_2\text{O}_3$ nanofibers was almost entirely covered when the zirconia loading was 50%. The elemental distribution mapping of the $\text{Al}_2\text{O}_3@\text{SO}_4^{2-}/\text{ZrO}_2\text{-}50\%$ sample was further conducted to determine the distribution of Zr, Al and S elements. The results present in Fig. 6 verified that these emerging irregular square nanoparticles were attributed to zirconia particles and densely covered the surface of the support to become zirconia coating coated on $\gamma\text{-Al}_2\text{O}_3$ nanofibers. Meanwhile, the distribution of S elements on the sample was also identified by Fig. 6e, signifying that the sulfur species were retained on the catalyst driven by sulfonation treatment and high-temperature calcination. Furthermore, the stand-alone $\text{SO}_4^{2-}/\text{ZrO}_2$ appeared a different morphology that the catalyst was well dispersed as nanoparticles with a clear grain boundary, and the particle size of this catalyst was observed to be significantly larger than that of the zirconia present on the $\text{Al}_2\text{O}_3@\text{SO}_4^{2-}/\text{ZrO}_2$ catalyst, which was consistent with the XRD results above. Altogether, supported by these results, it was evident that the envisaged structure, constructed by sulfated zirconia coated on the surface of $\gamma\text{-Al}_2\text{O}_3$ support, of the novel $\text{Al}_2\text{O}_3@\text{SO}_4^{2-}/\text{ZrO}_2$ composite catalyst was successfully formed.

The N_2 adsorption-desorption isotherms and pore size distribution plots of $\gamma\text{-Al}_2\text{O}_3$ cat, $\text{SO}_4^{2-}/\text{Al}_2\text{O}_3$ and $\text{Al}_2\text{O}_3@\text{SO}_4^{2-}/\text{ZrO}_2$ with various zirconia loading are shown in Fig. 7. The textural properties of these samples, such as specific surface area, pore volume and pore diameter, were analyzed and the relevant data are listed in Table 4. As observed in Fig. 7a, all isotherms corresponding to these catalysts were identified as the representative type IV isotherm with a hysteresis loop according to the IUPAC classification system, indicating the presence of mesopores in these catalysts. The appearance of the hysteresis loop in the N_2 adsorption-desorption isotherms, as the characteristic nature of mesoporous materials, is associated with capillary condensation occurring in the mesopores of the sample [41,42]. Interestingly, significant differences in hysteresis loops of these samples were found. It was apparent that the onset of the hysteresis loop of the $\gamma\text{-Al}_2\text{O}_3$ cat was located at about $P/P_0 = 0.65$, while that of the hysteresis loop of the $\text{SO}_4^{2-}/\text{Al}_2\text{O}_3$ was shifted to a lower relative pressure of $P/P_0 = 0.45$, which could be ascribed to changes in the pore structure. As exhibited in Fig. 7b, the $\gamma\text{-Al}_2\text{O}_3$ cat showed a broad pore size distribution ranging from 3 nm to 20 nm, while the $\text{SO}_4^{2-}/\text{Al}_2\text{O}_3$ contained relatively smaller pores dominantly distributed in the range of 3–9 nm, reflecting that original mesoporous with larger pore diameter were destroyed and broken into smaller pores owing to sulfonation treatment with H_2SO_4 .

Table 3

Crystallite size in (101) direction of the stand-alone $\text{SO}_4^{2-}/\text{ZrO}_2$ and $\text{Al}_2\text{O}_3@\text{SO}_4^{2-}/\text{ZrO}_2$ catalysts with different zirconia loading.

Sample	^a Crystallite size (nm)
$\text{SO}_4^{2-}/\text{ZrO}_2$	11.7
$\text{Al}_2\text{O}_3@\text{SO}_4^{2-}/\text{ZrO}_2\text{-}20\%$	5.2
$\text{Al}_2\text{O}_3@\text{SO}_4^{2-}/\text{ZrO}_2\text{-}30\%$	5.8
$\text{Al}_2\text{O}_3@\text{SO}_4^{2-}/\text{ZrO}_2\text{-}40\%$	6.2
$\text{Al}_2\text{O}_3@\text{SO}_4^{2-}/\text{ZrO}_2\text{-}50\%$	6.6
$\text{Al}_2\text{O}_3@\text{SO}_4^{2-}/\text{ZrO}_2\text{-}60\%$	6.7

^aThe crystallite size of the sample was calculated by Scherrer's equation: $D = K \cdot \lambda / (\beta \cdot \cos\theta)$.

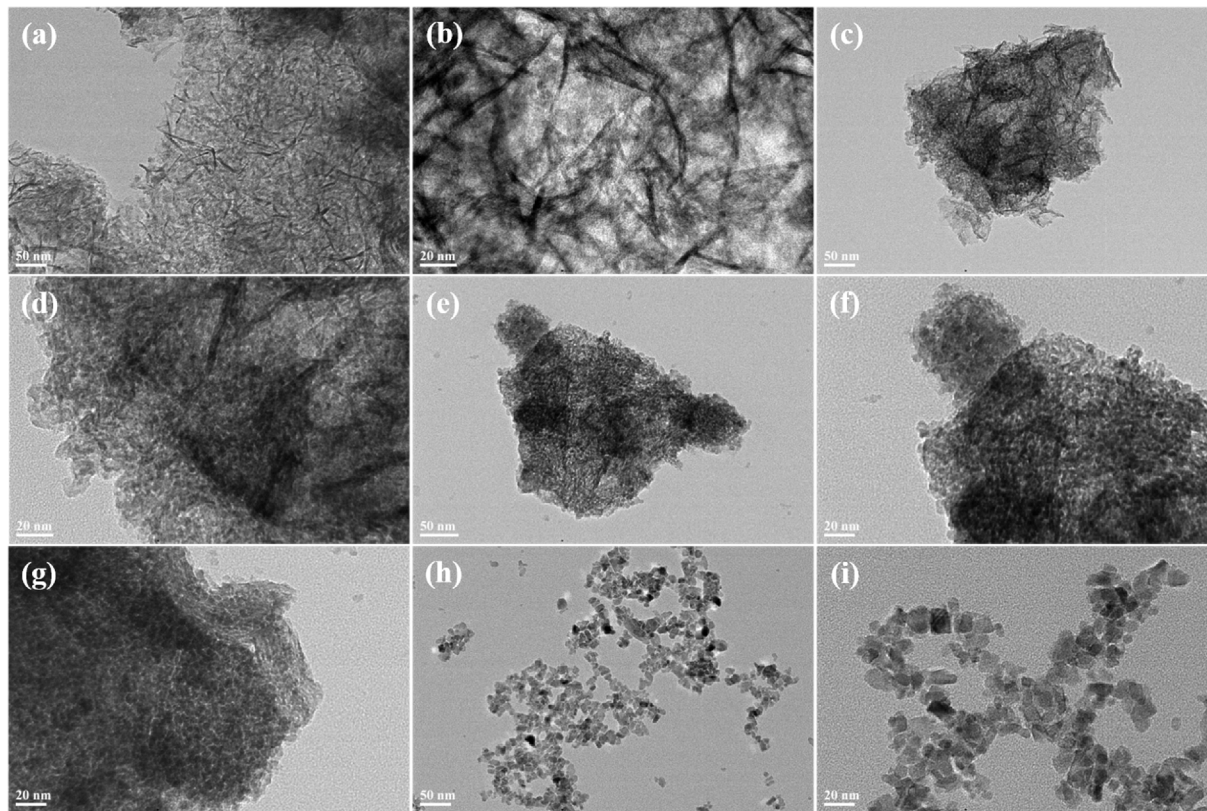


Fig. 5. HR-TEM images of (a, b) $\text{SO}_4^{2-}/\text{Al}_2\text{O}_3$, (c,d) $\text{Al}_2\text{O}_3@\text{SO}_4^{2-}/\text{ZrO}_2\text{-}30\%$, (e, f, g) $\text{Al}_2\text{O}_3@\text{SO}_4^{2-}/\text{ZrO}_2\text{-}50\%$ and (h, i) the stand-alone $\text{SO}_4^{2-}/\text{ZrO}_2$.

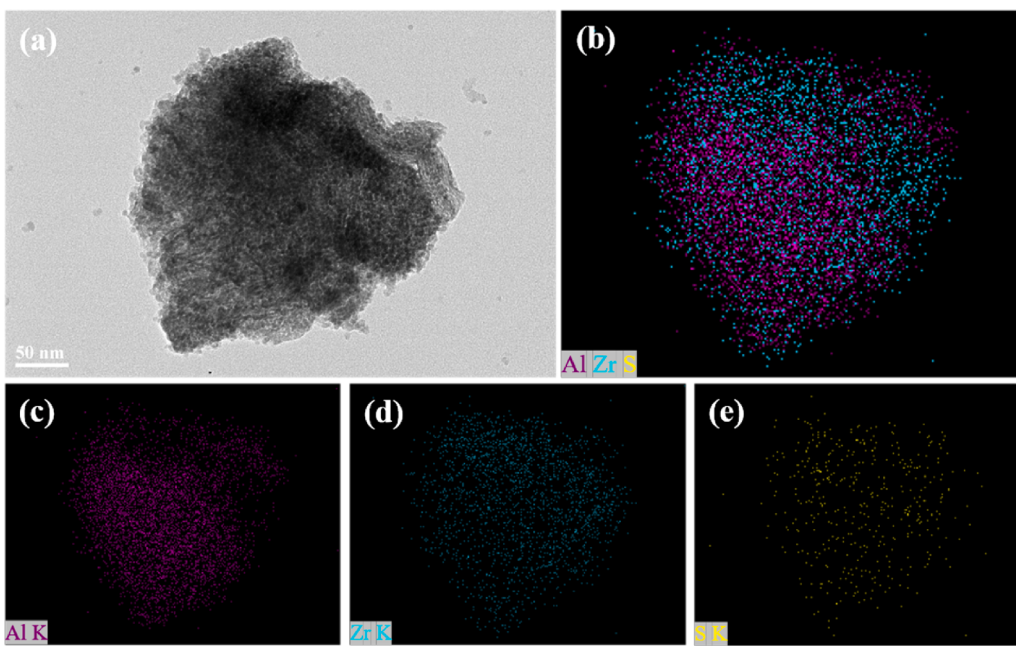


Fig. 6. HR-TEM image and corresponding elemental distribution mapping of (a) $\text{Al}_2\text{O}_3@\text{SO}_4^{2-}/\text{ZrO}_2\text{-}50\%$. (b) Al + Zr + S combined elemental mapping. (c) Al elemental mapping. (d) Zr elemental mapping. (e) S elemental mapping.

Additionally, for $\gamma\text{-Al}_2\text{O}_3$ cat and $\text{SO}_4^{2-}/\text{Al}_2\text{O}_3$, the hysteresis loops of the two samples could be assigned to the H3 type, whereas isotherms of all these $\text{Al}_2\text{O}_3@\text{SO}_4^{2-}/\text{ZrO}_2$ samples displayed the type H4 hysteresis loops. Studies [43,44] have shown that the type H3 hysteresis loop is attributed to slit-like pores derived from the interparticle porosity of the plate or fiber-like particles, and the type H4 hysteresis loop is

characteristic of narrow slit-like pores. Consequently, this observed difference in the hysteresis loop suggested that the pore size of $\text{Al}_2\text{O}_3@\text{SO}_4^{2-}/\text{ZrO}_2$ catalysts tended to become smaller than that of the $\text{SO}_4^{2-}/\text{Al}_2\text{O}_3$ catalyst, which was also supported by the pore size distribution of these catalysts in Fig. 7b. It could be ascribed to the coating of sulfated zirconia nanoparticles on the surface of the $\gamma\text{-Al}_2\text{O}_3$ support, as

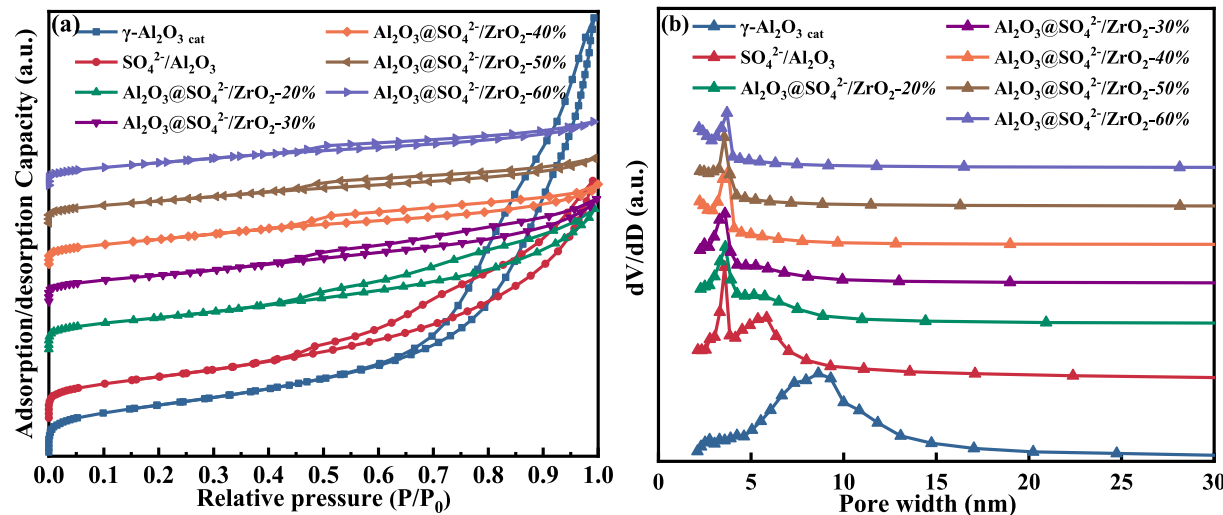


Fig. 7. (a) N₂ adsorption-desorption isotherms for Al₂O₃ support samples and Al₂O₃@SO₄²⁻/ZrO₂ catalysts with different zirconia loading and (b) the corresponding pore size distribution plots derived from the desorption isotherm of each sample.

Table 4

Textural properties of Al₂O₃ support samples and Al₂O₃@SO₄²⁻/ZrO₂ catalysts with different zirconia loading.

Sample	Sulfur content (wt%)	S _{BET} (m ² /g)	Pore volume (cm ³ /g)	Pore diameter (nm)
γ -Al ₂ O ₃ cat	–	267.5	0.969	11.3
SO ₄ ²⁻ /Al ₂ O ₃	–	213.7	0.544	7.2
Al ₂ O ₃ @SO ₄ ²⁻ /ZrO ₂ -20%	3.73	189.1	0.320	6.1
Al ₂ O ₃ @SO ₄ ²⁻ /ZrO ₂ -30%	3.61	161.4	0.231	5.4
Al ₂ O ₃ @SO ₄ ²⁻ /ZrO ₂ -40%	3.46	156.6	0.176	4.7
Al ₂ O ₃ @SO ₄ ²⁻ /ZrO ₂ -50%	3.19	143.2	0.153	4.5
Al ₂ O ₃ @SO ₄ ²⁻ /ZrO ₂ -60%	2.68	139.5	0.152	4.5

has been revealed by TEM characterization. The quantitative data in Table 4 further demonstrated that not only the pore size but also the pore volume and specific surface area of the Al₂O₃@SO₄²⁻/ZrO₂ composite catalysts were significantly decreased. To illustrate, as the zirconia loading raised from 20% to 60%, increasing sulfated zirconia nanoparticles accumulated and coated on the surface of the support, inducing the specific surface area of the catalyst to progressively decrease from 189.1 m²/g to 139.5 m²/g accompanied by the decline in pore volume from 0.320 cm³/g to 0.152 cm³/g and the decrease in pore diameter from 6.1 nm to 4.5 nm. Still, benefiting from the large specific surface area provided by the support and the loading of zirconia on it, such novel Al₂O₃@SO₄²⁻/ZrO₂ composite catalyst possessed a larger specific surface area than the bulk sulfated zirconia calcined at 650 °C, whose specific surface area was typically 80–110 m²/g [16,19,45,46].

The FT-IR spectra of as-synthesized Al₂O₃@SO₄²⁻/ZrO₂ catalysts with different zirconia loading were detected for the determination of the nature of surface sulfate species generated from sulfonation treatment. As plotted in Fig. 8, intense absorption bands positioned around 1049, 1080, 1148, 1226 and 1267 cm⁻¹, attributed to the chelating bidentate sulfate ion coordinated to metal cations [47,48], could be observed in spectra of all Al₂O₃@SO₄²⁻/ZrO₂ catalysts. Among them, the band detected at 1049 cm⁻¹ was associated with the symmetric stretching vibration of S-O bonds, while those at 1080, 1148, 1226 and 1267 cm⁻¹ arose from asymmetric stretching vibrations of S=O bonds [36,49–53]. Moreover, another intense absorption band centered at 1630 cm⁻¹

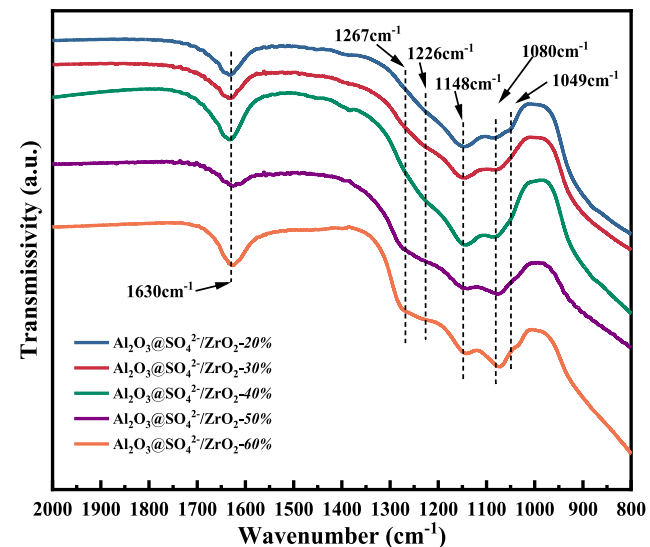


Fig. 8. FT-IR spectra of as-synthesized Al₂O₃@SO₄²⁻/ZrO₂ catalysts with different zirconia loading.

corresponded to the bending vibration ($\delta_{\text{H-O-H}}$) of water associated with the sulfate group [54,55]. Hence, these results further demonstrated that the sulfate ions were successfully retained on the surface of the Al₂O₃@SO₄²⁻/ZrO₂ catalyst after high-temperature calcination and coordinated with zirconium cations, which could be indispensably responsible for the development of acid sites.

The acidic properties of Al₂O₃@SO₄²⁻/ZrO₂ catalysts with different zirconia loading were investigated by NH₃-TPD. As presented in Fig. 9, the NH₃-TPD curves corresponding to all these Al₂O₃@SO₄²⁻/ZrO₂ catalysts displayed similar patterns, and each curve could be divided into three peaks. The first ammonia desorption peaks observed in the temperature region of 100–300 °C could be assigned to weak acid sites. Meanwhile, the other two peaks in the temperature region of 300–550 °C and 550–650 °C were attributed to moderate and strong acid sites, respectively [48,56–58]. The fitted peak area of the ammonia desorption peak can be taken as an indicator for estimating the amount of acid sites of the catalyst since the constant mass of the sample was used in each experiment [59]. Accordingly, it could be well acknowledged that the Al₂O₃@SO₄²⁻/ZrO₂ catalyst possessed abundant acid sites,

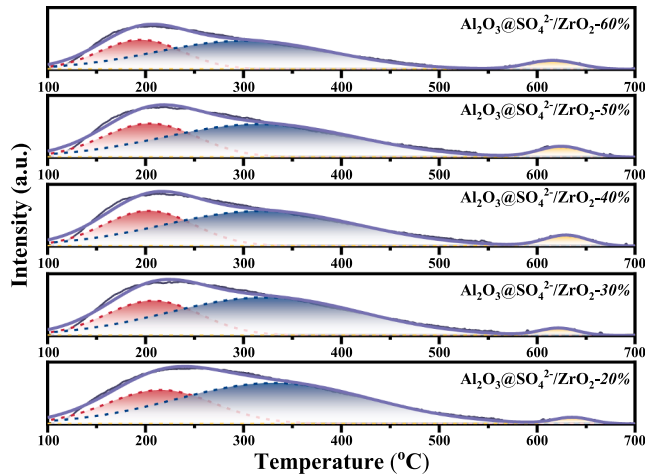


Fig. 9. NH₃-TPD curves of as-synthesized Al₂O₃@SO₄²⁻/ZrO₂ catalysts with different zirconia loading and the deconvoluted peaks of NH₃-TPD curves.

which could contribute to the excellent catalytic activity of the catalyst. By increasing the zirconia loading from 20% to 60%, the peak areas corresponding to weak and moderate acid sites were gradually decreased, indicating the decline in the amount of both two acid sites of these as-synthesized catalysts. It has been reported that the aluminum species introduced into the sulfated zirconia catalyst can promote the improvement in the content of sulfur species onto the catalyst [23,38,60], which has also been verified in our previous study [18], and the acidity of the catalyst dominantly depends on the content of surface sulfur species [15,61–63]. In the present study, on the one hand, the increase of zirconia loading inevitably caused a decrease in aluminum concentration; on the other hand, zirconia was coated on the surface of Al₂O₃. Such promoting effect of Al species was inevitably weakened,

which in turn gave rise to a decrease in the surface sulfur species content of the as-synthesized catalyst. As a result, the amount of acid sites of the catalyst were reduced. As listed in Table 4, the order of these samples' actual surface sulfur content was $\text{Al}_2\text{O}_3@\text{SO}_4^2/\text{ZrO}_2-20\%$ > $\text{Al}_2\text{O}_3@\text{SO}_4^2/\text{ZrO}_2-30\%$ > $\text{Al}_2\text{O}_3@\text{SO}_4^2/\text{ZrO}_2-40\%$ > $\text{Al}_2\text{O}_3@\text{SO}_4^2/\text{ZrO}_2-50\%$ > $\text{Al}_2\text{O}_3@\text{SO}_4^2/\text{ZrO}_2-60\%$, and the total amount of acid sites of the catalyst were positively correlated with the sulfur content. On the contrary, an overall enhancement trend in strong acid sites was observed with increasing the zirconia loading of the catalyst, which might be ascribed to more strong acid sites arose from sulfated zirconia coated on the support and the strong interaction between aluminum and zirconium.

Interestingly, it could be noticed that the catalytic performances of these $\text{Al}_2\text{O}_3@\text{SO}_4^{2-}/\text{ZrO}_2$ catalysts were not in parallel relationship with the total acid sites amount of catalysts, implying that the catalytic performance was not predominantly determined by the acid sites amount of the catalyst. To further understand the acid type of the $\text{Al}_2\text{O}_3@\text{SO}_4^{2-}/\text{ZrO}_2$ catalyst, the Brønsted (B) and Lewis (L) acid sites on the catalyst surface were distinguished by taking advantage of the *in situ* pyridine FTIR spectroscopy with pyridine as the probe molecule. The Py-FTIR spectra of these representative catalysts were provided in Fig. 10, where the spectra of two support samples (Al_2O_3 cat and $\text{SO}_4^{2-}/\text{Al}_2\text{O}_3$) and the stand-alone $\text{SO}_4^{2-}/\text{ZrO}_2$ were also collected to help gain insight into the effect of zirconia loading on the acid type. As demonstrated in Fig. 10, the characteristic adsorption peaks centered at around 1540, 1490 and 1450 cm^{-1} were observed in the spectra of $\text{Al}_2\text{O}_3@\text{SO}_4^{2-}/\text{ZrO}_2$, $\text{SO}_4^{2-}/\text{ZrO}_2$, $\text{SO}_4^{2-}/\text{Al}_2\text{O}_3$ and Al_2O_3 cat. Among them, the peaks at 1540 cm^{-1} can be assigned to the vibration of pyridine molecules coordinated to Brønsted acid sites on the catalyst surface, and the peaks at 1450 cm^{-1} take the indication of interactions between pyridine molecules and Lewis acid sites of the catalyst [64–68]. At the same time, the peaks located at 1490 cm^{-1} are attributed to the synergistic effect between Brønsted and Lewis acid sites present on the catalyst [62,69]. Moreover, the spectra recorded at 200°C and 450°C in the

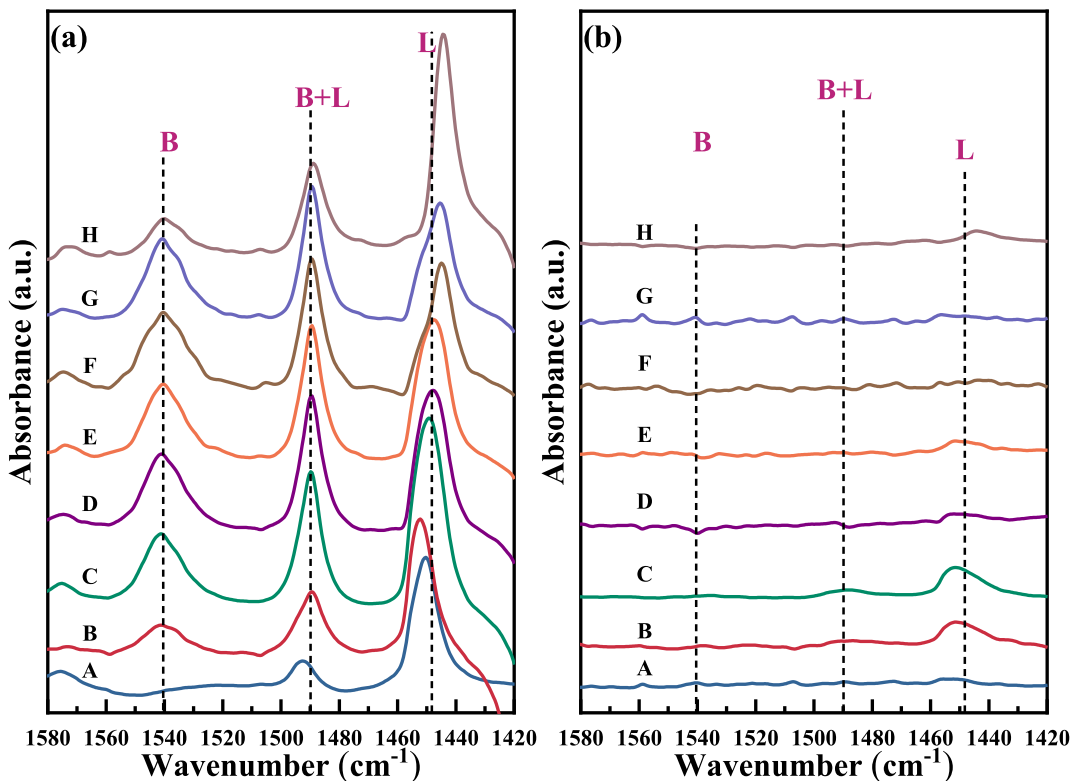


Fig. 10. Py-FTIR spectra of these representative catalysts desorbed at (a) 200 °C and (b) 450 °C. (A) γ -Al₂O₃ cat; (B) SO₄²⁻/Al₂O₃; (C) Al₂O₃@SO₄²⁻/ZrO₂-20%; (D) Al₂O₃@SO₄²⁻/ZrO₂-30%; (E) Al₂O₃@SO₄²⁻/ZrO₂-40%; (F) Al₂O₃@SO₄²⁻/ZrO₂-50%; (G) Al₂O₃@SO₄²⁻/ZrO₂-60%; (H) SO₄²⁻/ZrO₂.

S. Wang et al.

Separation and Purification Technology 308 (2023) 122731

measurement are related to the total and strong Brønsted (or Lewis) acid sites of the catalyst, respectively, and the weak acid sites are determined by their difference [70]. Consequently, these spectra identified the presence of Brønsted and Lewis acid sites on these catalysts, but the difference in the absorbance of characteristic adsorption peaks at 1540, 1490 and 1450 cm⁻¹ signified that these catalysts possessed different amounts of Brønsted and Lewis acid sites.

The amount of Brønsted and Lewis acid sites on these as-synthesized catalysts was calculated according to the following equations, guided by the Lambert-Beer law [66].

$$\text{Content}_L = 1.42 \times \left(A_L R^2 / W \right)$$

$$\text{Content}_B = 1.88 \times \left(A_B R^2 / W \right)$$

where $\text{Content}_{L(B)}$ refers to the amount of Lewis or Brønsted acid sites on the catalyst samples (μmol·g⁻¹ catalyst); $A_{L(B)}$ indicates the integrated areas of Lewis or Brønsted peaks (cm⁻¹); meanwhile, R and W are the radius (cm) and weight (mg) of the sample wafer, respectively.

The corresponding quantitative results are summarized in Table 5. As observed in Fig. 10 and Table 5, it could be found that all these Al₂O₃@SO₄²⁻/ZrO₂ catalysts contained abundant Brønsted and Lewis acid sites. Even though both Brønsted and Lewis acid sites were also observed to be contained in SO₄²⁻/ZrO₂, the acid sites of this catalyst were dominated by Lewis acid sites (69 μmol·g⁻¹), along with little Brønsted acid sites (23 μmol·g⁻¹). Apparently, the amount of Brønsted acid sites on the Al₂O₃@SO₄²⁻/ZrO₂ catalyst with zirconia loading varying from 20% to 60% was significantly higher than that of the stand-alone SO₄²⁻/ZrO₂, and the former was about 2–3 times more than the latter. It has been testified in Fig. 10 and Table 5 that no Brønsted acid sites could be detected on the γ-Al₂O₃ cat catalyst, synthesized by the direct calcination of pseudo-boehmite nanoparticles, and only Lewis acid sites were present on the sample. In addition, although the sulfonation treatment could allow the generation of Brønsted acid sites on the surface of SC₄²⁻/Al₂O₃, the catalyst still possessed a smaller amount of Brønsted acid sites than the Al₂O₃@SO₄²⁻/ZrO₂ catalyst, even for comparison with Al₂O₃@SO₄²⁻/ZrO₂-20% with the minimum Brønsted acid sites among the series of Al₂O₃@SO₄²⁻/ZrO₂ catalysts. Thus, these findings implicated that a synergistic interaction was performed between Al₂O₃ as the support and ZrO₂ as the coating on the generation of acid sites, which could promote the enhancement of Brønsted acid sites on such a novel composite catalyst. Furthermore, for the series of Al₂O₃@SO₄²⁻/ZrO₂ catalysts, the catalyst displayed a decreasing trend in the total amount of acid sites, with the zirconia loading increasing from 20% to 60%, which was in line with the findings of NH₃-TPD measurement.

Concerning the amount of two types of acid sites, it was noteworthy that the distribution of Brønsted and Lewis acid sites on these Al₂O₃@SO₄²⁻/ZrO₂ catalysts was considerably affected by zirconia loading. Since strong Brønsted or Lewis acid site properties, determined

by Py-FTIR measurement, of Al₂O₃@SO₄²⁻/ZrO₂ catalysts were found to be similar, as well as all these catalysts contained much fewer strong acid sites than weak acid sites, the amount of total Brønsted and Lewis acid sites of the catalyst was mainly paid attention. Table 5 shows that the amount of Lewis acid sites dramatically declined with an increment in zirconia loading, while the amount of Brønsted acid sites appeared the opposite trend. In detail, the total amount of Brønsted acid sites on Al₂O₃@SO₄²⁻/ZrO₂ was progressively increased from 48 μmol·g⁻¹ to 64 μmol·g⁻¹ in the range of zirconia loading from 20% to 50% and became dominant on the catalyst. Then it slightly decreased to 59 μmol·g⁻¹ when the zirconia loading was increased to 60%. Accordingly, the ratio of T_B/T_L almost increased with the increment in zirconia loading of the catalyst. Previous studies [15,18,20,61,62,71] have suggested that the amount of Brønsted acid sites of the sulfated zirconia catalyst is highly determined by the content of active sulfur species retained on the catalyst. Table 4 has testified that the sulfur content decreased as zirconia loading increased. However, an increase in the amount of Brønsted acid sites with increasing the loading of zirconia was observed. In contrast to previous studies, the amount of Brønsted acid sites on Al₂O₃@SO₄²⁻/ZrO₂ did not display a dominant dependence on the sulfur retention of the catalyst in the current study, which might be attributable to the synergistic effect between Al species and Zr species on the promotion of Brønsted acid sites. The Al₂O₃@SO₄²⁻/ZrO₂ catalyst with low zirconia loading possessed a relatively small amount of Brønsted acid sites but contained more Lewis acid sites. It could be explained by the fact that SO₄²⁻/Al₂O₃ components would be present in the catalyst due to the insufficient coating of the support by zirconia, as confirmed by the detectable of γ-Al₂O₃ crystalline phase in XRD patterns. Noticeably, a positive correlation between the catalytic performance of the Al₂O₃@SO₄²⁻/ZrO₂ catalyst and the amount of Brønsted acid sites was found, in which the conversion of olefins almost changed with the amount of Brønsted acid sites variation trend, as shown in Figure S1. It suggested that the Brønsted acid sites were in favor of the excellent catalytic performance of the catalyst.

3.2. The fabrication mechanism of the Al₂O₃@SO₄²⁻/ZrO₂ catalyst

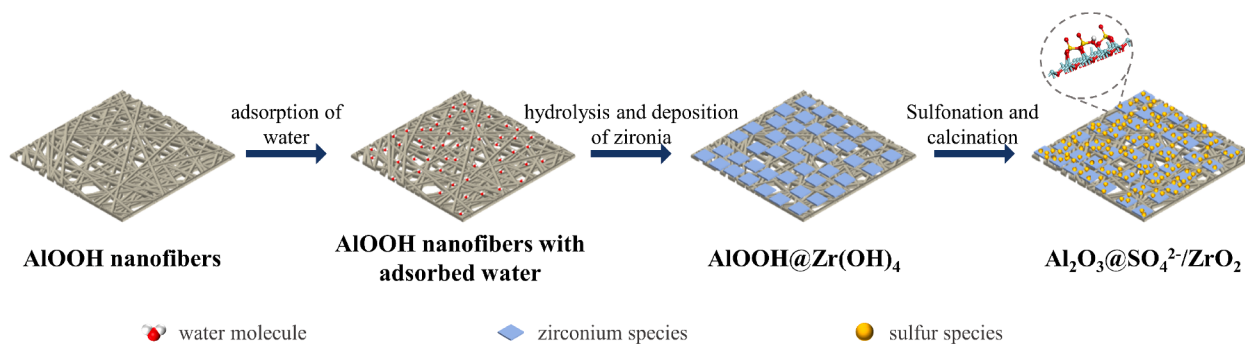
Based on the preceding analysis, it could be well known that the Al₂O₃@SO₄²⁻/ZrO₂ catalyst with a structure of sulfated zirconia coated on γ-alumina was successfully synthesized and performed outstanding catalytic performance in olefins removal from reforming aromatics. Combined with characterization results, the fabrication mechanism of Al₂O₃@SO₄²⁻/ZrO₂ was proposed, as illustrated in Fig. 11. Due to the significant difference in polarity between CH₃(CH₂)₃OH ($\mu = 3.7$ D) and H₂O ($\mu = 10.2$ D), the hydrophobic property is appeared by n-butanol [72,73]. In the step of pre-adsorption of water, the added water molecules would preferentially interact with abundant hydroxyl groups provided by pseudo-boehmite and attach to the surface of pseudo-boehmite nanofibers. Accordingly, the hydrolysis of zirconium (IV) n-butoxide occurred on the surface of pseudo-boehmite nanofibers rather than in the n-butanol solution, which could be proved by the absence of stand-alone zirconia particles in TEM morphologies of the Al₂O₃@SO₄²⁻/

Table 5

Bronsted and Lewis acid properties derived from Py-FTIR spectra of γ-Al₂O₃ cat, SO₄²⁻/Al₂O₃, SO₄²⁻/ZrO₂ and Al₂O₃@SO₄²⁻/ZrO₂ catalysts with different zirconia loading.^b

Sample	Total	Lewis acid sites			Bronsted acid sites			T _B /T _L
		Total	weak	strong	Total	weak	strong	
γ-Al ₂ O ₃ cat	81	81	78	3	—	—	—	—
SO ₄ ²⁻ /Al ₂ O ₃	107	78	66	12	29	27	2	0.372
Al ₂ O ₃ @SO ₄ ²⁻ /ZrO ₂ -20%	138	90	76	14	48	46	2	0.533
Al ₂ O ₃ @SO ₄ ²⁻ /ZrO ₂ -30%	118	65	62	3	53	52	1	0.815
Al ₂ O ₃ @SO ₄ ²⁻ /ZrO ₂ -40%	115	59	56	3	56	54	2	0.949
Al ₂ O ₃ @SO ₄ ²⁻ /ZrO ₂ -50%	113	49	45	4	64	63	1	1.306
Al ₂ O ₃ @SO ₄ ²⁻ /ZrO ₂ -60%	106	47	44	3	59	58	1	1.255
SO ₄ ²⁻ /ZrO ₂	92	69	65	4	23	23	—	0.333

^bUnits = μmol·g⁻¹.

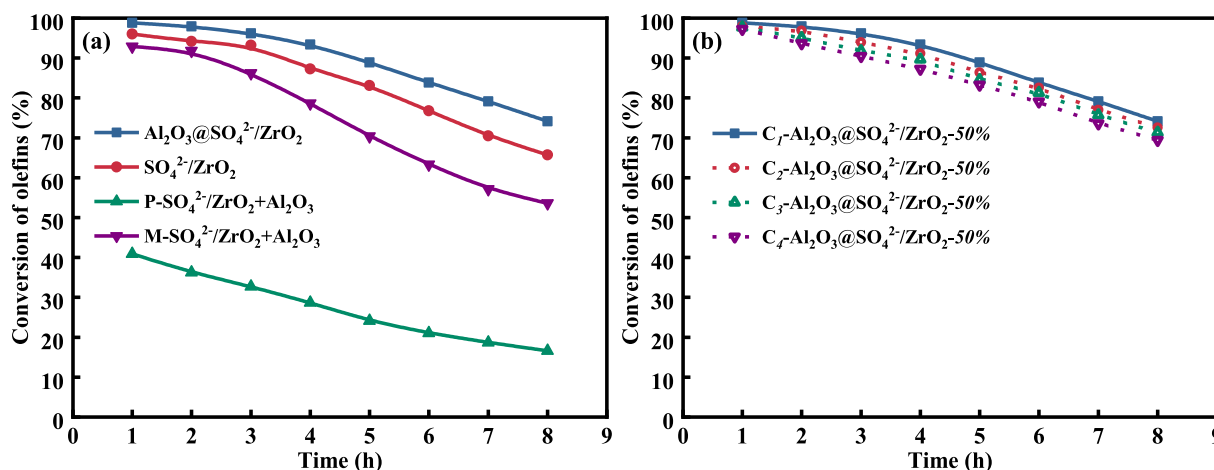
Fig. 11. Schematic illustration of the fabrication mechanism of $\text{Al}_2\text{O}_3@\text{SO}_4^{2-}/\text{ZrO}_2$.

ZrO_2 catalyst. Then the amorphous zirconium hydroxide was deposited onto the surface of pseudo-boehmite nanofibers, and $\text{AlOOH}@\text{Zr}(\text{OH})_4$ composites were formed. Moreover, the integrity of the zirconia coating onto the support surface could be governed by increasing the zirconia loading of the catalyst in the synthesis process. After sulfonation and calcination treatment, the retained sulfur species presented as chelating bidentate sulfate ion coordinated to zirconia coated on the support, as shown in Fig. 11. The sulfate ion coordinated to zirconia was of vital significance to the generation of acid sites for the catalyst, as confirmed by Py-FTIR measurement. Owing to the strong electron-withdrawing effect of covalent sulfate anion, the surface Zr atoms can be induced by the sulfate ion to lose electrons and perform unsaturated coordination states, thereby contributing to generating Lewis acid sites. Besides, the protonation of water or hydroxy group absorbed on Lewis acid sites could be further promoted due to the electron-withdrawing effect displayed by the unsaturated surface Zr^{n+} , thus, Brønsted acid sites are developed [62,71].

3.3. Comparison between the $\text{Al}_2\text{O}_3@\text{SO}_4^{2-}/\text{ZrO}_2$ catalyst, aluminum-free sulfated zirconia, and aluminum-modified catalysts synthesized by other strategies

Given the outstanding catalytic performance performed by $\text{Al}_2\text{O}_3@\text{SO}_4^{2-}/\text{ZrO}_2$ -50% in the intermittent reaction, it was chosen as the representative sample to further investigate the catalytic stability of the novel $\text{Al}_2\text{O}_3@\text{SO}_4^{2-}/\text{ZrO}_2$ catalyst by carrying out the continuous reaction for olefins removal in the fixed-bed tubular microreactor. Additionally, $\text{SO}_4^{2-}/\text{ZrO}_2$, as the representative sample of aluminum-free sulfated zirconia, while $\text{P-SO}_4^{2-}/\text{ZrO}_2 + \text{Al}_2\text{O}_3$ and $\text{M-SO}_4^{2-}/\text{ZrO}_2 + \text{Al}_2\text{O}_3$, as the representative sample of aluminum-modified

catalysts synthesized by other strategies, were also investigated for comparison with $\text{Al}_2\text{O}_3@\text{SO}_4^{2-}/\text{ZrO}_2$. It was worth mentioning that the liquid hourly space velocity for the evaluation was amplified from 1 h^{-1} adopted in industrial processes to 30 h^{-1} , aiming to highlight differences in the catalytic stability of these catalysts in a short time. As shown in Fig. 12a, the $\text{Al}_2\text{O}_3@\text{SO}_4^{2-}/\text{ZrO}_2$ catalyst demonstrated the most outstanding catalytic stability over the whole test. The conversion of olefins over the $\text{Al}_2\text{O}_3@\text{SO}_4^{2-}/\text{ZrO}_2$ catalyst was nearly maintained above 80% within eight hours, which was significantly higher than that of the other three catalysts. Although better catalytic activity and stability could be obtained by the $\text{SO}_4^{2-}/\text{ZrO}_2$ catalyst when compared with the other typical heterogeneous catalysts for removing olefins from aromatics (such as industrial clay, modified industrial clay and USY zeolite), the overall catalytic performance of $\text{SO}_4^{2-}/\text{ZrO}_2$ was still inferior to that of $\text{Al}_2\text{O}_3@\text{SO}_4^{2-}/\text{ZrO}_2$, as verified by Figure S2 and Fig. 12. Apparently, the $\text{P-SO}_4^{2-}/\text{ZrO}_2 + \text{Al}_2\text{O}_3$ catalyst showed the poorest catalytic performance among these four representative catalysts, in which the conversion of olefins was much lower than that displayed by the $\text{Al}_2\text{O}_3@\text{SO}_4^{2-}/\text{ZrO}_2$ catalyst within whole eight hours, indicating that the introduction of such a large amount of aluminum species into the zirconia via the co-precipitation method could reduce the catalytic performance of the catalyst. According to our previous study [18], the content of aluminum species, incorporated into the catalyst with the co-precipitation method, dramatically affects the promoting effect of Al on the physicochemical properties of as-synthesized aluminum-modified catalysts. In the case of low aluminum content ($\text{Al/Zr} < 7.5 \text{ mol\%}$), the tetragonal zirconia phase and acid sites of the resultant catalyst can be promoted by the Al promoter, giving rise to the enhancement in the catalytic performance compared with the bulk sulfated zirconia. However, when the incorporation of Al is at a high level, the crystallization

Fig. 12. (a) The catalytic stability in olefins removal of $\text{Al}_2\text{O}_3@\text{SO}_4^{2-}/\text{ZrO}_2$, $\text{SO}_4^{2-}/\text{ZrO}_2$, $\text{P-SO}_4^{2-}/\text{ZrO}_2 + \text{Al}_2\text{O}_3$ and $\text{M-SO}_4^{2-}/\text{ZrO}_2 + \text{Al}_2\text{O}_3$. (b) The reusability of $\text{Al}_2\text{O}_3@\text{SO}_4^{2-}/\text{ZrO}_2$.

and growth of zirconia are restricted by increasing aluminum species concentrated in the lattice gap of zirconia, playing adverse effects on the textural properties and formation of acid sites, which is detrimental to the catalytic performance of the catalyst. In the synthesis of $\text{Al}_2\text{O}_3@\text{SO}_4^{2-}/\text{ZrO}_2$, zirconia was embedded on the surface of γ - Al_2O_3 support by the chemical liquid deposition method. Even at such high aluminum content, amorphous zirconium hydroxide deposit on the support surface could crystallize into zirconia with the tetragonal phase after calcination, and the surface properties of the resultant sample tend to be close to that of pristine zirconia owing to the accumulating and coating of zirconia particles on the support. Moreover, the aluminum-modified catalyst synthesized via the milling method was also not feasible for adding such high content of aluminum. As shown in Fig. 12a, a weakening in catalytic activity and stability, instead of improved catalytic performance than pristine $\text{SO}_4^{2-}/\text{ZrO}_2$, was observed over the $\text{M}-\text{SO}_4^{2-}/\text{ZrO}_2 + \text{Al}_2\text{O}_3$ sample. In short, it was of great advantage to synthesize the $\text{Al}_2\text{O}_3@\text{SO}_4^{2-}/\text{ZrO}_2$ catalyst with a high aluminum content by coating ZrO_2 on γ - Al_2O_3 . This synthesis strategy could not only facilitate less zirconia contained in the as-synthesized catalyst than bulk sulfated zirconia to reduce manufacturing costs but also promote the superior catalytic activity and stability of the catalyst.

3.4. Reusability of the $\text{Al}_2\text{O}_3@\text{SO}_4^{2-}/\text{ZrO}_2$ catalyst

The reusability, as one of the advantages of heterogeneous catalysts, is critical to the overall lifetime and industrial feasibility of the catalyst. In an attempt to estimate the reusability of the novel $\text{Al}_2\text{O}_3@\text{SO}_4^{2-}/\text{ZrO}_2$ catalyst, consecutive reaction-regeneration cycles of the $\text{Al}_2\text{O}_3@\text{SO}_4^{2-}/\text{ZrO}_2-50\%$ catalyst in the removal of trace olefins from reforming aromatics were carried out. After each catalytic performance evaluation, the reacted catalyst was collected from the tubular microreactor and dried in an oven at 120 °C. As presented in Fig. 13a, the color of the fresh catalyst has changed from the initial white to black after reaction, which was considered to be resulted from carbon deposition. By comparing the TGA curves of the fresh and spent catalyst, it was clearly that the spent catalyst displayed an obvious weight loss in the range of 350 °C and 550 °C, attributed to the decomposition of carbon deposit. Therefore, the dried spent catalyst sample was calcined in the air at 550 °C for reusing in the next cycle, and each catalytic reaction was conducted under the same reaction conditions as the first cycle. Note, $\text{C}_n-\text{Al}_2\text{O}_3@\text{SO}_4^{2-}/\text{ZrO}_2-50\%$ was used to label the sample for the reusability test, in which n denoted the number of the catalytic reaction cycle. The results in Fig. 12b identified that the conversion of olefins decreased slightly after consecutive reaction-regeneration cycles. The $\text{Al}_2\text{O}_3@\text{SO}_4^{2-}/\text{ZrO}_2-50\%$ catalyst was efficient up to 4 cycles giving the conversion was still maintained at about 98%-70% throughout each

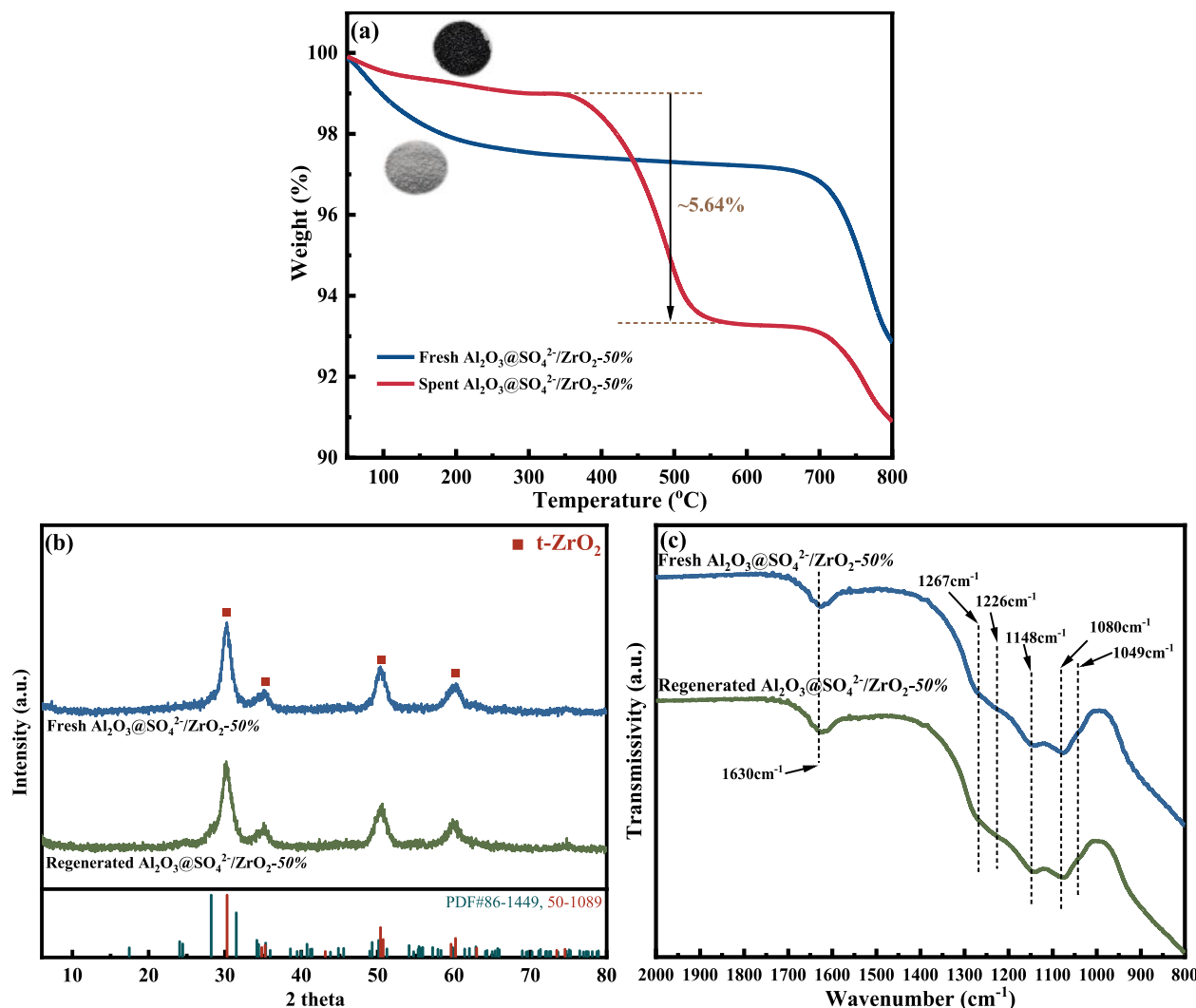


Fig. 13. (a) Thermogravimetric analysis of the fresh and spent $\text{Al}_2\text{O}_3@\text{SO}_4^{2-}/\text{ZrO}_2-50\%$; (b) Powder XRD patterns and (c) FTIR spectra of the fresh $\text{Al}_2\text{O}_3@\text{SO}_4^{2-}/\text{ZrO}_2-50\%$ and regenerated sample after four cycles.

evaluation even after being used 4 times.

To understand the slight decrease in catalytic activity after each cycle, the properties of the fresh and regenerated catalyst were compared by conducting XRD, N₂ adsorption-desorption isotherms, EA, FT-IR, and Py-FTIR characterization. As seen in Table 6, the specific surface area and pore volume of the catalyst decreased dramatically after the long-term reaction, accompanied by an increase in the average pore diameter, mainly caused by carbon deposition during the reaction process. As a result, numerous accessible surfaces and acid sites of the catalyst would be covered, which, in turn, resulted in the continuous decline with the reaction time of olefin conversion during each cycle. (The N₂ adsorption-desorption isotherms for the fresh, spent and regenerated Al₂O₃@SO₄²⁻/ZrO₂-50% catalyst could be seen in Figure S3.) Fortunately, textural properties of Al₂O₃@SO₄²⁻/ZrO₂-50% could be greatly recovered by high-temperature calcination at 550 °C, facilitating the re-exposure of active sites for reactions. This might explain the fact that the catalytic activity of the spent catalyst could be restored to a level close to that of the fresh one with a slight decline. Additionally, according to CHNS analysis of the catalyst, it was found that the content of sulfur species retained on the catalyst slightly decreased from 3.19% (fresh catalyst) to 2.64% (regenerated catalyst). Our previous study [18] has shown that bulk sulfated zirconia suffers from dramatic sulfur loss, given that a noticeable decline in the sulfur content of the catalyst from 2.70% to 1.50% after 2 cycles can be observed. Even if sulfur loss could still be detected on the Al₂O₃@SO₄²⁻/ZrO₂-50%, it was negligible compared to that of bulk sulfated zirconia, which could be beneficial to alleviate the decrease of acid sites. To compare acidic properties of the fresh and regenerated Al₂O₃@SO₄²⁻/ZrO₂-50%, the two samples were further characterized by Py-FTIR. The Py-FTIR spectra are provided in Figure S4, and the corresponding quantitative results are summarized in Table 7. It was apparent from Table 7 that the acidity of the catalyst was only slightly decreased after 4 consecutive reaction-regeneration cycles, owing to the alleviation of sulfur loss, as suggested above. The decrease in the acidity of the catalyst could further account for the slight decrease in the conversion of olefins after consecutive reaction-regeneration cycles since acidic properties of catalysts played a crucial role in catalytic performance. Furthermore, the crystalline structure and surface sulfur species of the fresh Al₂O₃@SO₄²⁻/ZrO₂-50%, as well as the regenerated Al₂O₃@SO₄²⁻/ZrO₂-50%, were compared. As presented in Fig. 13b, it was clear from XRD patterns of the two samples that there were no apparent changes between the crystalline structure of the fresh catalyst and the regenerated catalyst after 4 consecutive reaction-regeneration cycles, which illustrated that the tetragonal zirconia of the catalyst was stable during the reaction and regeneration process. The results provided in Fig. 13c imply that the FTIR spectra of the regenerated catalyst were almost similar to those of the fresh one, and the intensity of the five S-related absorption bands barely significantly changed. Altogether, it could be concluded that the Al₂O₃@SO₄²⁻/ZrO₂-50% catalyst was reusable and displayed excellent reusability, favoring the potential for industrial applications.

3.5. Reaction mechanism analysis

The reaction mechanism for olefins removal from reforming aromatics over the Al₂O₃@SO₄²⁻/ZrO₂ catalyst was investigated as well. In view of the complexity of the raw reforming aromatics obtained from the industrial unit, a model oil was prepared with the mass fractions of toluene, *m*-xylene and 1-octene being about 45%, 45% and 10%, respectively. The reaction with the model oil as feedstock and Al₂O₃@SO₄²⁻/ZrO₂-50% as catalyst was carried out under the same conditions as control experiments for optimization of Al₂O₃@SO₄²⁻/ZrO₂ synthesis. After the reaction, the feedstock oil and reacted oil were analyzed by GC-MS technology, and the results were provided in Fig. 14a and 14b. Obviously, the disappearance of the characteristic peak attributed to 1-octene, accompanied by the appearance of some new peaks at around 14 min, was observed by comparing the gas chromatography of the reacted and feedstock oil. The mass spectrometry analysis in Figure S5 confirmed that these new peaks at 13.8, 14.0, 14.2 and 14.5 min could be assigned to C₁₅H₂₄ (*m/z* = 204), generated by alkylation of 1-octene with toluene. Meanwhile, the other three peaks at 14.6, 14.9 and 15.4 mins were verified as products with a chemical formula of C₁₆H₂₆ (*m/z* = 218), arising from alkylation of 1-octene with *m*-xylene. Moreover, the molecular structures of these alkylation products are shown in Fig. 14b. Thus, it was evident that the conversion of olefins was owing to the Friedel-Crafts alkylation of olefins with aromatics catalyzed by the Al₂O₃@SO₄²⁻/ZrO₂ catalyst. Some researchers [5–7,18,74] have proposed that the alkylation of olefins with aromatics is based on the carbonium ion mechanism, in which Brønsted and Lewis acid sites perform a synergistic effect. Particularly, Brønsted acid sites of the catalyst are conducive to the protonation of olefins to form more carbonium ions, promoting the electrophilic substitution reaction with the benzene ring of aromatics. As proved above, the Al₂O₃@SO₄²⁻/ZrO₂-50% catalyst exhibited superior catalytic activity in olefins conversion, ascribing to its higher Brønsted acidity, as well as abundant Lewis acidity, compared to the Al₂O₃@SO₄²⁻/ZrO₂ catalyst with other zirconia loadings.

Consequently, guided by the carbonium ion mechanism and combined with the results of this work, a possible reaction pathway for the alkylation of olefins with aromatics over the Al₂O₃@SO₄²⁻/ZrO₂ catalyst was proposed and presented in Fig. 14c. Due to the strong electron-donating properties of the benzene ring, aromatics are preferentially adsorbed on Lewis acid sites. Meanwhile, Brønsted acid sites of the catalyst induce the protonation of olefin molecules adsorbed on them to produce carbonium ions, which can further attack the benzene ring of aromatics to generate alkylation products. Then Lewis acid sites will be recovered by the desorption of these alkyl aromatic hydrocarbons and participate in the following reaction cycle. In addition, to balance the positive charge, the benzene ring of aromatics adsorbed on Lewis acid sites will release protons, which can help recover Brønsted acid sites to continue interacting with olefin molecules in the subsequent cycle.

4. Conclusions

With the advantage of the chemical liquid deposition method, Zr species were selectively deposited and accumulated on the surface of alumina, avoiding the homogeneous distribution of Zr species and Al species that generally arose out of incorporating Al species by co-precipitation method or milling method. Accordingly, the crystallization and growth of amorphous zirconium hydroxide to form zirconia crystal could not be intensely hindered even at exceedingly high aluminum content. The novel Al₂O₃@SO₄²⁻/ZrO₂ composites with a structure composed of sulfated zirconia-coated γ-alumina were successfully synthesized based on this strategy and applied as efficient catalysts for purification of reforming aromatics. Zirconia particles dispersed on the support tended to be present as a small particle size driven by the interaction between Al₂O₃ and ZrO₂, which contributed to stabilizing catalytically active tetragonal zirconia. Besides, the

Table 6
Textural properties of the fresh, spent and regenerated Al₂O₃@SO₄²⁻/ZrO₂-50%.

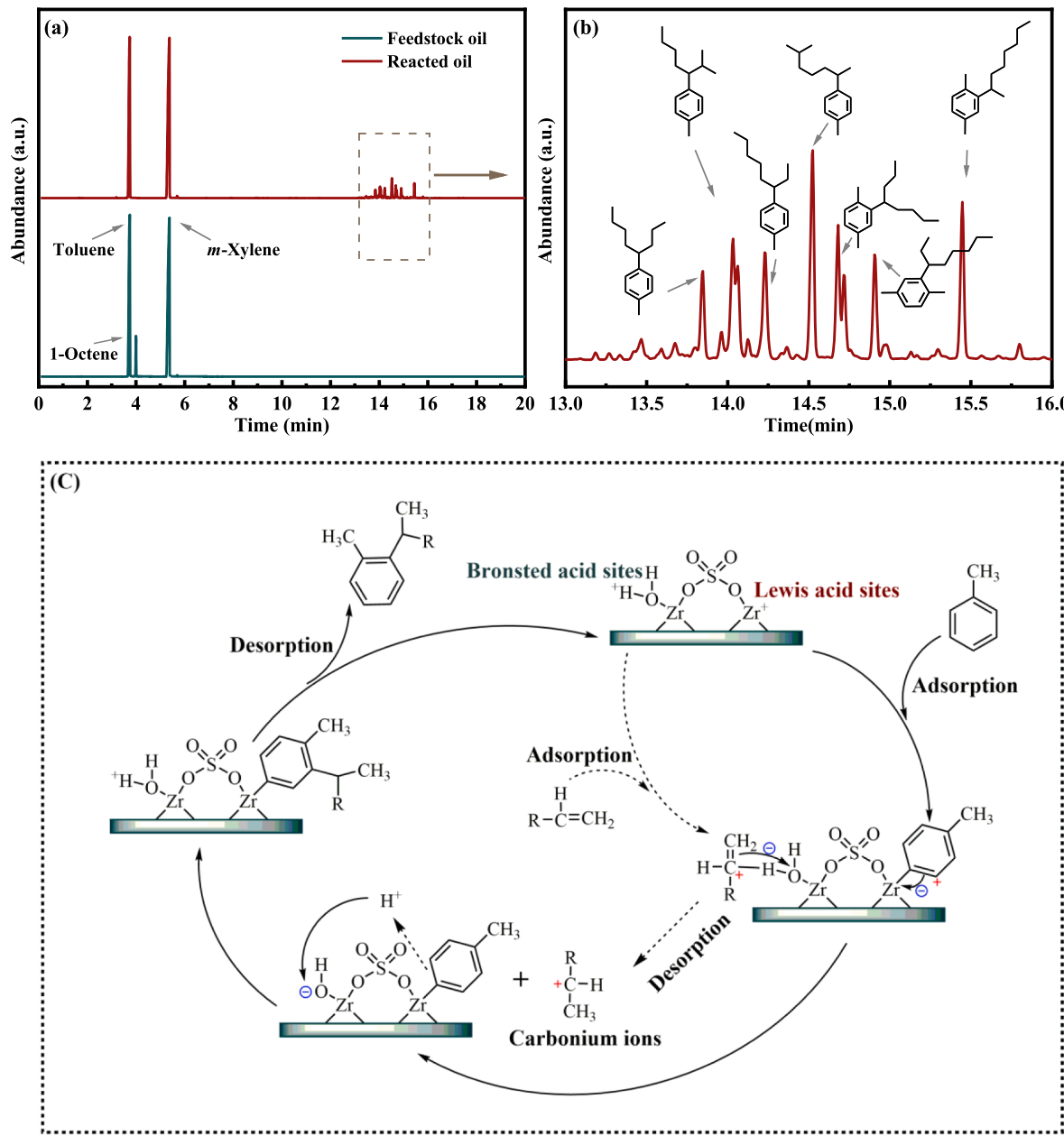
Sample	Sulfur content (wt%)	S _{BET} (m ² /g)	Pore volume (cm ³ /g)	Pore diameter (nm)
F ^c -Al ₂ O ₃ @SO ₄ ²⁻ /ZrO ₂ -50%	3.19	143.2	0.153	4.5
S ^d -Al ₂ O ₃ @SO ₄ ²⁻ /ZrO ₂ -50%	–	42.1	0.084	6.1
R ^e -Al ₂ O ₃ @SO ₄ ²⁻ /ZrO ₂ -50%	2.64	126.9	0.154	4.5

F^c = Fresh, S^d = Spent, R^e = Regenerated.

Table 7

Brønsted and Lewis acid properties derived from Py-FTIR spectra of the fresh and regenerated $\text{Al}_2\text{O}_3@\text{SO}_4^2/\text{ZrO}_2$ -50%.

Sample	Total	Lewis acid sites			Brønsted acid sites			T_B/T_L
		Total	weak	strong	Total	weak	strong	
F- $\text{Al}_2\text{O}_3@\text{SO}_4^2/\text{ZrO}_2$ -50%	113	49	45	4	64	63	1	1.306
R- $\text{Al}_2\text{O}_3@\text{SO}_4^2/\text{ZrO}_2$ -50%	99	46	45	1	53	53	–	1.152

Fig. 14. (a) GC-MS analysis of model feedstock oil and reacted oil. (b) The zooming time from 13.0 min to 16 min of GC-MS analysis of reacted oil. (c) Proposed mechanistic pathway for alkylation of olefins with aromatics over the $\text{Al}_2\text{O}_3@\text{SO}_4^2/\text{ZrO}_2$ catalyst. (toluene as the representative).

introduction of Al also significantly promoted generating more Brønsted acid sites and alleviating sulfur loss of the $\text{Al}_2\text{O}_3@\text{SO}_4^2/\text{ZrO}_2$ catalyst. Through the optimization of synthesis variables, it can be well known that the optimal synthesis condition for the catalyst is sulfonation of the zirconium-aluminum composite precursor with 50% zirconia loading with 0.5 mol/L H_2SO_4 for 1 h followed by calcination at 650 °C, given the maximum olefins conversion of 93.78% in the intermittent reaction over the resultant catalyst.

Benefiting from the advantageous structural and acidic properties of $\text{Al}_2\text{O}_3@\text{SO}_4^2/\text{ZrO}_2$, the catalyst could perform the superior catalytic activity and long-term stability. Besides, the excellent reusability of $\text{Al}_2\text{O}_3@\text{SO}_4^2/\text{ZrO}_2$ was also confirmed, given the slight decline in catalytic activity after 4 consecutive reaction-regeneration cycles compared to that of the fresh catalyst ascribed to the stable tetragonal zirconia phase and the inhibited surface sulfur leaching. Based on GC-MS analysis, the alkylation pathway of olefins with aromatics over $\text{Al}_2\text{O}_3@\text{SO}_4^2/$

S. Wang et al.

Separation and Purification Technology 308 (2023) 122731

ZrO_2 was proposed, in which Lewis and Brønsted acid sites synergistically participate, and Brønsted acid sites could crucially facilitate the protonation of olefins to generate more carbonium ions for reaction. Accordingly, an effective strategy to synthesize high-aluminum-content sulfated zirconia with the preservation of excellent catalytic activity and stability was developed, thereby overcoming the inherent drawbacks of co-precipitation and milling methods. The $\text{Al}_2\text{O}_3@\text{SO}_4^{2-}/\text{ZrO}_2$ catalyst demonstrated broad application prospects in acid-catalyzed reactions to replace bulk sulfated zirconia synthesized by the conventional route.

CRediT authorship contribution statement

Sitan Wang: Conceptualization, Methodology, Software, Investigation, Writing – original draft. **Xuan Meng:** Validation, Formal analysis, Visualization, Software, Supervision. **Naiwang Liu:** Writing – review & editing. **Li Shi:** Writing – review & editing, Supervision.

Declaration of Competing Interest

The authors declare that they have no known competing financial interests or personal relationships that could have appeared to influence the work reported in this paper.

Data availability

No data was used for the research described in the article.

Acknowledgments

The authors sincerely and gratefully appreciate the National Science Foundation of China (NO.21808054) for providing the financial support to carry out our research.

Appendix A. Supplementary data

Supplementary data to this article can be found online at <https://doi.org/10.1016/j.seppur.2022.122731>.

References

- [1] C. Chen, W. Wu, X. Zeng, Z. Jiang, L. Shi, Study on several mesoporous materials catalysts applied to the removal of trace olefins from aromatics and commercial sidestream tests, *Ind. Eng. Chem. Res.* 48 (2009) 10359–10363.
- [2] H. Guo, H. Zhang, Q. Li, F. Peng, L. Xiong, C. Wang, A. Hu, S. Yao, X. Chen, Removal of olefins from reforming aromatic hydrocarbons over metal-halide-modified acid-activated palygorskite, *Energy Fuel* 34 (2020) 9463–9472.
- [3] J.-N. Luan, G.-L. Li, L. Shi, Study of Modified Clay and Its Industrial Testing in Aromatic Refining, *Ind. Eng. Chem. Res.* 50 (2011) 7150–7154.
- [4] R.R. Pawar, P. Sakaria, A. Bhatt, H.M. Mody, H.C. Bajaj, Catalytic activity of acid activated clay for removal of olefins from aromatic hydrocarbons by continuous method using fix bed reactor. in: 20th National Symposium on Catalysis-IIT-Chennai-India, 2010.
- [5] X. Pu, L. Shi, Commercial test of the catalyst for removal of trace olefins from aromatics and its mechanism, *Catal. Today* 212 (2013) 115–119.
- [6] X. Yao, T. Luo, T. Yin, S. Lou, X. Meng, N. Liu, L. Shi, Gas-assisted exfoliation montmorillonite into mono-layered nanosheets for the removal of olefins from aromatics, *Fuel* 306 (2021), 121720.
- [7] N. Liu, X. Pu, X. Wang, L. Shi, Study of alkylation on a Lewis and Brønsted acid hybrid catalyst and its industrial test, *Journal of Industrial Engineering, Chemistry* 20 (2014) 2848–2857.
- [8] G. Li, J. Luan, X. Zeng, L. Shi, Removal of trace olefins from aromatics over metal-halides-modified clay and its industrial test, *Ind. Eng. Chem. Res.* 50 (2011) 6646–6649.
- [9] X. Pu, N. Liu, Z. Jiang, L. Shi, Acidic and Catalytic Properties of Modified Clay for Removing Trace Olefin from Aromatics and Its Industrial Test, *Ind. Eng. Chem. Res.* 51 (2012) 13891–13896.
- [10] X. Pu, N. Liu, L. Shi, Acid Properties and Catalysis of USY Zeolite With Different Extra-Framework Aluminum Concentration, *Microporous Mesoporous Mater.* 201 (2015) 17–23.
- [11] J.K. Reddy, S. Lad, K. Mantri, J. Das, G. Raman, R.V. Jasra, Zeolite-based catalysts for the removal of trace olefins from aromatic streams, *Appl. Petrochem. Res.* 10 (2020) 107–114.
- [12] H. Yu, J. Zang, G. Liu, M. Hong, R. Chen, T. Chen, Acid-Modified Hierarchical Porous Rare-Earth-Containing Y Zeolite as a Highly Active and Stable Catalyst for Olefin Removal, *ACS Omega* 5 (2020) 18028–18034.
- [13] Y. Tian, X. Meng, L. Shi, Synthesis of SO_3^2- -functionalized ionic liquids and their novel application in removal of trace olefins from aromatics, *Ind. Eng. Chem. Res.* 52 (2013) 6655–6661.
- [14] Y. Sun, L. Shi, Removal of Trace Olefins from Aromatics at Room Temperature Using Pyridinium and Imidazolium Ionic Liquids, *Ind. Eng. Chem. Res.* 50 (2011) 9339–9343.
- [15] J. Liu, N. Liu, K. Ren, L. Shi, X. Meng, Sulfated zirconia synthesized in a one step solvent-free method for removal of olefins from aromatics, *Ind. Eng. Chem. Res.* 56 (2017) 7693–7699.
- [16] J. Yao, N. Liu, L. Shi, X. Wang, Sulfated zirconia as a novel and recyclable catalyst for removal of olefins from aromatics, *Catal. Commun.* 66 (2015) 126–129.
- [17] Q. Zhao, J. Liu, J. Yao, L. Shi, X. Wang, Purification of aromatics over a promising $\text{SO}_4^{2-}/\text{ZrO}_2$ catalyst, *Chin. Pet. Process Pe. Technol.* 18 (2016) 49.
- [18] S. Wang, T. Yin, X. Meng, N. Liu, L. Shi, Synthesis of Al-incorporated sulfated zirconia with improved and stabilized surface sulfur species for removal of trace olefins from aromatics, *Catal. Sci. Technol.* 12 (2022) 212–225.
- [19] N. Liu, X. Guo, A. Navrotsky, L. Shi, D. Wu, Thermodynamic complexity of sulfated zirconia catalysts, *J. Catal.* 342 (2016) 158–163.
- [20] S. Wang, X. Meng, N. Liu, L. Shi, Effective Catalyst for Removing Trace Olefins from Reforming Aromatics: Sulfated Zirconia with High Sulfur Content Synthesized by Sulfonation with Chlorosulfonic Acid, *Ind. Eng. Chem. Res.* 61 (2022) 5103–5116.
- [21] C.-C. Huang, C.-J. Yang, P.-J. Gao, N.-C. Wang, C.-L. Chen, J.-S. Chang, Characterization of an alkaline earth metal-doped solid superacid and its activity for the esterification of oleic acid with methanol, *Green Chem.* 17 (2015) 3609–3620.
- [22] K. Saravanan, B. Tyagi, R.S. Shukla, H. Bajaj, Esterification of palmitic acid with methanol over template-assisted mesoporous sulfated zirconia solid acid catalyst, *Appl. Catal. B* 172 (2015) 108–115.
- [23] Y. Zhang, T. Chen, G. Zhang, G. Wang, H. Zhang, Mesoporous Al-promoted sulfated zirconia as an efficient heterogeneous catalyst to synthesize isosorbide from sorbitol, *Appl. Catal. A* 562 (2018) 258–266.
- [24] W. Hua, Y. Xia, Y. Yue, Z. Gao, Promoting Effect of Al on $\text{SO}_4^{2-}/\text{M}_x\text{O}_y$ ($\text{M}=\text{Zr}, \text{Ti}, \text{Fe}$) Catalysts, *J. Catal.* 196 (2000) 104–114.
- [25] P. Canton, R. Olindo, F. Pinna, G. Strukul, P. Riello, M. Meneghetti, G. Cerrato, C. Morterra, A. Benedetti, Alumina-Promoted Sulfated Zirconia System: Structure and Microstructure Characterization, *Chem. Mater.* 13 (2001) 1634–1641.
- [26] C.-C. Hwang, C.-Y. Mou, Alumina-Promoted Sulfated Mesoporous Zirconia Catalysts, *J. Phys. Chem. C* 113 (2009) 5212–5221.
- [27] B.M. Reddy, G.K. Reddy, K.N. Rao, L. Katta, Influence of alumina and titania on the structure and catalytic properties of sulfated zirconia: Beckmann rearrangement, *J. Mol. Catal. A. Chem.* 306 (2009) 62–68.
- [28] B. Rahmani Vahid, N. Saghatoleslami, H. Nayebzadeh, J. Toghiani, Effect of alumina loading on the properties and activity of $\text{SO}_4^{2-}/\text{ZrO}_2$ for biodiesel production: Process optimization via response surface methodology, *J. Taiwan Inst. Chem. Eng.* 83 (2018) 115–123.
- [29] E. Liu, A.J. Locke, W.N. Martens, R.L. Frost, X. Yang, Fabrication of Macro-Mesoporous Zirconia-Alumina Materials with a One-Dimensional Hierarchical Structure, *Cryst. Growth Des.* 12 (2012) 1402–1410.
- [30] M.K. Mishra, B. Tyagi, R.V. Jasra, Effect of Synthetic Parameters on Structural, Textural, and Catalytic Properties of Nanocrystalline Sulfated Zirconia Prepared by Sol-Gel Technique, *Ind. Eng. Chem. Res.* 42 (2003) 5727–5736.
- [31] X. Sang, L. Zhang, H. Wang, D. He, L. Deng, S. Huang, J. Wang, Y. Luo, Influence of synthetic parameters on structural and catalytic properties of sulfated zirconia nanoparticles prepared by employing sulfate-containing anion surfactants via one-step route, *Powder Technol.* 253 (2014) 590–595.
- [32] N. Tangchupong, W. Khaodee, B. Jongsomjit, N. Laosiripojana, P. Praserthdam, S. Assabumrungrat, Effect of calcination temperature on characteristics of sulfated zirconia and its application as catalyst for isosynthesis, *Fuel Process. Technol.* 91 (2010) 121–126.
- [33] Y. Zhang, W. Wong, K. Yung, Biodiesel production via esterification of oleic acid catalyzed by chlorosulfonic acid modified zirconia, *Appl. Energy* 116 (2014) 191–198.
- [34] Y.R. Smith, K. Joseph Antony Raj, V. Subramanian, B. Viswanathan, Sulfated $\text{Fe}_2\text{O}_3\text{-TiO}_2$ synthesized from ilmenite ore: A visible light active photocatalyst, *Colloids and Surfaces A: Physicochemical and Engineering Aspects*, 367 (2010) 140–147.
- [35] Q.H. Xia, K. Hidajat, S. Kawi, Effect of ZrO_2 Loading on the Structure, Acidity, and Catalytic Activity of the $\text{SO}_4^{2-}/\text{ZrO}_2/\text{MCM}-41$ Acid Catalyst, *J. Catal.* 205 (2002) 318–331.
- [36] H. Li, H. Chu, X. Ma, G. Wang, F. Liu, M. Guo, W. Lu, S. Zhou, M. Yu, Efficient heterogeneous acid synthesis and stability enhancement of UiO-66 impregnated with ammonium sulfate for biodiesel production, *Chem. Eng. J.* 408 (2021), 127277.
- [37] R.C. Garvie, The Occurrence of Metastable Tetragonal Zirconia as a Crystallite Size Effect, *J. Phys. Chem.* 69 (1965) 1238–1243.
- [38] Z. Ma, X. Meng, C. Yang, N. Liu, Y. Zhang, L. Shi, Study of High-Aluminum-Content Sulfated Zirconia: Influence of Aluminum Content and Washing, *Ind. Eng. Chem. Res.* 56 (2017) 5598–5606.
- [39] P.D.L. Mercera, J.G.V. Ommen, E.B.M. Doesburg, A.J. Burggraaf, J.R.H. Ross, Zirconia as a Support for Catalysts Evolution of the Texture and Structure on Calcination in Air, *Appl. Catal.* 57 (1990) 127–148.

- [40] W.-H. Chen, H.-H. Ko, A. Sakthivel, S.-J. Huang, S.-H. Liu, A.-Y. Lo, T.-C. Tsai, S.-B. Liu, A solid-state NMR, FT-IR and TPD study on acid properties of sulfated and metal-promoted zirconia: Influence of promoter and sulfation treatment, *Catal. Today* 116 (2006) 111–120.
- [41] S. Shen, P.S. Chow, S. Kim, K. Zhu, R.B.H. Tan, Synthesis of carboxyl-modified rod-like SBA-15 by rapid co-condensation, *J. Colloid Interface Sci.* 321 (2008) 365–372.
- [42] C. Yan, S. Zheng, N. Chen, S. Yuan, Y. Chen, B. Li, Y. Zhang, Sulfated zirconia catalysts supported on mesoporous Mg-SBA-15 with different morphologies for highly efficient conversion of fructose to 5-hydroxymethylfurfural, *Microporous Mesoporous Mater.* 328 (2021), 111507.
- [43] A. Martínez, G. Prieto, J. Rollán, Nanofibrous γ -Al₂O₃ as support for Co-based Fischer-Tropsch catalysts: Pondering the relevance of diffusional and dispersion effects on catalytic performance, *J. Catal.* 263 (2009) 292–305.
- [44] M. Thommes, K. Kaneko, A.V. Neimark, J.P. Olivier, F. Rodriguez-Reinoso, J. Rouquerol, K.S.W. Sing, Physisorption of gases, with special reference to the evaluation of surface area and pore size distribution (IUPAC Technical Report), 87 (2015) 1051–1069.
- [45] J. Oh, S. Yang, C. Kim, I. Choi, J.H. Kim, H. Lee, Synthesis of biolubricants using sulfated zirconia catalysts, *Appl. Catal. A* 455 (2013) 164–171.
- [46] J. Zhao, Y. Yue, W. Hua, H. He, Z. Gao, Catalytic activities and properties of sulfated zirconia supported on mesostructured γ -Al₂O₃, *Appl. Catal. A* 336 (2008) 133–139.
- [47] Y. Kim, J. Kim, H.W. Kim, T.-W. Kim, H.J. Kim, H. Chang, M.B. Park, H.-J. Chae, Sulfated Tin Oxide as Highly Selective Catalyst for the Chlorination of Methane to Methyl Chloride, *ACS Catal.* 9 (2019) 9398–9410.
- [48] A. Sinhamahapatra, N. Sutradhar, M. Ghosh, H.C. Bajaj, A.B. Panda, Mesoporous sulfated zirconia mediated acetalization reactions, *Appl. Catal. A* 402 (2011) 87–93.
- [49] T. Yamaguchi, T. Jin, K. Tanabe, Structure of acid sites on sulfur-promoted iron oxide, *J. Phys. Chem.* 90 (1986) 3148–3152.
- [50] V.G. Deshmukh, Y.G. Adewuyi, Mesoporous nanocrystalline sulfated zirconia synthesis and its application for FFA esterification in oils, *Appl. Catal. A* 462 (2013) 196–206.
- [51] X. Zhang, A.I.M. Rabee, M. Isaacs, A.F. Lee, K. Wilson, Sulfated Zirconia Catalysts for D-Sorbitol Cascade Cyclodehydration to Isosorbide: Impact of Zirconia Phase, *ACS Sustain. Chem. Eng.* 6 (2018) 14704–14712.
- [52] F. Haase, J. Sauer, The Surface Structure of Sulfated Zirconia: Periodic ab Initio Study of Sulfuric Acid Adsorbed on ZrO₂(101) and ZrO₂(001), *J. Am. Chem. Soc.* 120 (1998) 13503–13512.
- [53] D. Huang, S. Chen, S. Ma, X. Chen, Y. Ren, M. Wang, L. Ye, L. Zhang, X. Chen, Z.-P. Liu, B. Yue, H. He, Determination of acid structures on the surface of sulfated monoclinic and tetragonal zirconia through experimental and theoretical approaches, *Catalysis, Sci. Technol.* 12 (2022) 596–605.
- [54] P. Wang, S. Wang, Y. Yue, H. Zhu, T. Wang, X. Bao, In Situ Diffuse Reflectance Infrared Fourier Transform Spectroscopy Investigations on the Evolution of Surface and Catalysis Properties of Alumina-Promoted Sulfated Zirconia during n-Butane Isomerization, *Ind. Eng. Chem. Res.* 59 (2020) 704–712.
- [55] T. Witoon, T. Permsirivach, N. Kanjanasontorn, C. Akkaraphatworn, A. Seubsa, K. Faungnawakij, C. Warakulwit, M. Chareonpanich, J. Limtrakul, Direct synthesis of dimethyl ether from CO₂ hydrogenation over Cu-ZnO-ZrO₂/SO₄²⁻-ZrO₂ hybrid catalysts: effects of sulfur-to-zirconia ratios, *Catalysis, Sci. Technol.* 5 (2015) 2347–2357.
- [56] K. Na, S. Alayoglu, R. Ye, G.A. Somorjai, Effect of Acidic Properties of Mesoporous Zeolites Supporting Pt Nanoparticles on Hydrogenative Conversion of Methylcyclopentane, *J. Am. Chem. Soc.* 136 (2014) 17207–17212.
- [57] A. Wang, J. Wang, C. Lu, M. Xu, J. Lv, X. Wu, Esterification for biofuel synthesis over an eco-friendly and efficient kaolinite-supported SO₄²⁻/ZnAl₂O₄ macroporous solid acid catalyst, *Fuel* 234 (2018) 430–440.
- [58] Y. Lyu, Y. Liu, L. Xu, X. Zhao, Z. Liu, X. Liu, Z. Yan, Effect of ethanol on the surface properties and n-heptane isomerization performance of Ni/SAPO-11, *Appl. Surf. Sci.* 401 (2017) 57–64.
- [59] Y. Wu, L. Qin, G. Zhang, L. Chen, X. Guo, M. Liu, Porous Solid Superacid SO₄²⁻/Fe₂_xZr_xO₃ Fenton Catalyst for Highly Effective Oxidation of X-3B under Visible Light, *Ind. Eng. Chem. Res.* 52 (2013) 16698–16708.
- [60] W. Hua, Y. Xia, Y. Yue, Z. Gao, Promoting Effect of Al on SO₄²⁻/M_xO_y (M=Zr, Ti, Fe) Catalysts, *J. Catal.* 196 (2000) 104–114.
- [61] K. Föttinger, K. Zorn, H. Vinek, Influence of the sulfate content on the activity of Pt containing sulfated zirconia, *Appl. Catal. A* 284 (2005) 69–75.
- [62] H. Wang, Y. Li, F. Yu, Q. Wang, B. Xing, D. Li, R. Li, A Stable Mesoporous Super-Acid Nanocatalyst for Eco-Friendly Synthesis of Biodiesel, *Chem. Eng. J.* 364 (2019) 111–122.
- [63] D.-D. Li, X.-Y. Leng, X.-F. Wang, H.-B. Yu, W.-Q. Zhang, J. Chen, J.-Q. Lu, M.-F. Luo, Unraveling the promoting roles of sulfate groups on propane combustion over Pt-SO₄²⁻/ZrO₂ catalysts, *J. Catal.* 407 (2022) 322–332.
- [64] W. Ciptonugroho, M.G. Al-Shaal, J.B. Mensah, R. Palkovits, One pot synthesis of WO₃/mesoporous-ZrO₂ catalysts for the production of levulinic-acid esters, *J. Catal.* 340 (2016) 17–29.
- [65] H. Li, T. Yang, Z. Fang, Biomass-derived mesoporous Hf-containing hybrid for efficient Meerwein-Ponndorf-Verley reduction at low temperatures, *Appl Catal B* 227 (2018) 79–89.
- [66] C.A. Emeis, Determination of Integrated Molar Extinction Coefficients for Infrared Absorption Bands of Pyridine Adsorbed on Solid Acid Catalysts, *J. Catal.* 141 (1993) 347–354.
- [67] K. Saravanan, B. Tyagi, R.S. Shukla, H.C. Bajaj, Esterification of palmitic acid with methanol over template-assisted mesoporous sulfated zirconia solid acid catalyst, *Appl. Catal. B* 172–173 (2015) 108–115.
- [68] Y. Feng, M. Zuo, T. Wang, W. Jia, X. Zhao, X. Zeng, Y. Sun, X. Tang, T. Lei, L. Lin, Efficient synthesis of glucose into 5-hydroxymethylfurfural with SO₄²⁻/ZrO₂ modified H⁺ zeolites in different solvent systems, *J. Taiwan Inst. Chem. Eng.* 96 (2019) 431–438.
- [69] J. Gardy, A. Osatiashvili, O. Céspedes, A. Hassanpour, X. Lai, A.F. Lee, K. Wilson, M. Rehan, A magnetically separable SO₄²⁻/Fe-Al-TiO₂ solid acid catalyst for biodiesel production from waste cooking oil, *Appl. Catal. B* 234 (2018) 268–278.
- [70] S. Zhang, Y. Gong, L. Zhang, Y. Liu, T. Dou, J. Xu, F. Deng, Hydrothermal treatment on ZSM-5 extrudates catalyst for methanol to propylene reaction: Finely tuning the acidic property, *Fuel Process. Technol.* 129 (2015) 130–138.
- [71] C. Morterra, G. Cerrato, V. Bolis, Lewis and Brønsted acidity at the surface of sulfate-doped ZrO₂ catalysts, *Catal. Today* 17 (1993) 505–515.
- [72] J. Tang, K.K. Sirkar, S. Majumdar, Pervaporative dehydration of concentrated aqueous solutions of selected polar organics by a perfluoropolymer membrane, *Sep. Purif. Technol.* 175 (2017) 122–129.
- [73] E. Liu, A.J. Locke, R.L. Frost, W.N. Martens, Sulfated fibrous ZrO₂/Al₂O₃ core and shell nanocomposites: A novel strong acid catalyst with hierarchically macro-mesoporous nanostructure, *J. Mol. Catal. A Chem.* 353–354 (2012) 95–105.
- [74] Y. Liu, Q. Liu, K. Sun, S. Zhao, Y.D. Kim, Y. Yang, Z. Liu, Z. Peng, Identification of the Encapsulation Effect of Heteropolyacid in the Si-Al Framework toward Benzene Alkylation, *ACS Catal.* 12 (2022) 4765–4776.